NASA TECHNICAL MEMORANDUM

NASA TM X-1095

NASA TM X-1095

SUPERSONIC CHARACTERISTICS OF BOTH LAUNCH AND FLYBACK CONFIGURATIONS OF A VTO REUSABLE LAUNCH VEHICLE

by Robert J. McGhee and P. Kenneth Pierpont

Langley Research Center
Langley Station, Hampton, Va.

NATIONAL AERONAUTICS AND SPACE ADMINISTRATION • WASHINGTON, D. C. • MAY 1965

NASA TM X-1095

SUPERSONIC CHARACTERISTICS OF BOTH LAUNCH AND FLYBACK CONFIGURATIONS OF A VTO REUSABLE LAUNCH VEHICLE

By Robert J. McGhee and P. Kenneth Pierpont

Langley Research Center
Langley Station, Hampton, Va.

NATIONAL AERONAUTICS AND SPACE ADMINISTRATION

SUPERSONIC CHARACTERISTICS OF BOTH LAUNCH AND FLYBACK CONFIGURATIONS OF A VTO REUSABLE LAUNCH VEHICLE*

By Robert J. McGhee and P. Kenneth Pierpont
Langley Research Center

SUMMARY

An investigation has been conducted in the Langley Unitary Plan wind tunnel to determine the longitudinal and lateral-directional stability for a vertical-take-off launch vehicle and its fixed-wing reusable first stage. In addition, control effectiveness, effects of vertical-tail arrangements, and a semisubmerged flyback engine nacelle are indicated for the reusable first stage. The complete launch vehicle was tested at angles of attack from -4° to 16°, sideslip angles of 0° and 4°, and Mach numbers of 2.36, 2.96, and 4.63. The first-stage reusable booster was tested at angles of attack from -4° to 35° for the same Mach numbers and sideslip angles as the complete launch vehicle. Test Reynolds numbers per foot varied from approximately 2×10^6 to 3×10^6.

From the estimated center-of-gravity location in flight during the launch trajectory, the longitudinal and lateral center of pressure of the launch vehicle are well rearward of the estimated center of gravity for all Mach numbers at an angle of attack of 0°.

The pitching-moment curves for the first-stage winged reusable booster were nonlinear and were characterized by a large range of lift coefficients with nominal stability. Outboard mounted vertical tails employing 15° of outboard cant provided significant improvement in longitudinal stability throughout the Mach number range of the investigation. Positive longitudinal stability coupled with small changes in stability with Mach number are indicated near maximum lift-drag ratio. Large wing-tip mounted vertical tails employing 5° of toe-in provided positive directional stability. Elevon effectiveness and longitudinal stability both decreased with upward elevon deflections. Rudder effectiveness decreased with increasing Mach number and angle of attack. Differential roll-control effectiveness increased with angle of attack but decreased with Mach number; however, the Mach number deterioration was considerably less at higher angles of attack.

*Title, Unclassified.

INTRODUCTION

The interest in future manned space flight missions suggests that winged reusable orbital launch vehicle systems may offer significant improvements from the standpoint of safety and reliability. The NASA Langley Research Center is investigating the aerodynamic characteristics of such launch vehicle systems. Results of investigations of an initial design of a large winged vertical-take-off reusable launch vehicle are indicated in reference 1.

The purpose of the present investigation was to provide aerodynamic characteristics of the complete two-stage vertical-take-off launch vehicle and the first-stage winged reusable booster at supersonic speeds. The first stage of the launch vehicle was completely redesigned from the test results of reference 1. Principal changes included a new wing planform and location as a result of a reassessment of the probable vehicle center of gravity and stability requirements, relocation and change in both area and planform of the vertical tails, and a relocation of the flyback turbine engines. Some effects on the first-stage reusable booster of vertical-tail arrangements and a semisubmerged flyback engine nacelle together with longitudinal, lateral, and directional control effectiveness are presented herein.

The tests were conducted in the Langley Unitary Plan wind tunnel at angles of attack from approximately -4° to 35° at Mach numbers of 2.36, 2.96, and 4.63. Data to derive stability characteristics were obtained at 0° and 4° of sideslip. The test Reynolds number per foot varied from approximately 2×10^6 to 3×10^6.

SYMBOLS

The aerodynamic data are reduced to standard coefficient form. All data for the launch vehicle are referred to the body axes. All lateral-directional and control data for the first-stage winged reusable booster are referred to the body axes, whereas the longitudinal data are referred to the stability axes. The moment reference for all data was selected to be 0.90 body diameter forward of the model base. All coefficients are referred to the body base area and body diameter.

C_N normal-force coefficient, $\dfrac{\text{Normal force}}{q_\infty S_{ref}}$

C_A axial-force coefficient, $\dfrac{\text{Total axial force}}{q_\infty S_{ref}}$

C_L lift coefficient, $\dfrac{\text{Lift}}{q_\infty S_{ref}}$

C_D drag coefficient, $\dfrac{\text{Total drag}}{q_\infty S_{ref}}$

C_m pitching-moment coefficient, $\frac{\text{Pitching moment}}{q_\infty S_{ref} D}$

C_l rolling-moment coefficient, $\frac{\text{Rolling moment}}{q_\infty S_{ref} D}$

C_n yawing-moment coefficient, $\frac{\text{Yawing moment}}{q_\infty S_{ref} D}$

C_Y side-force coefficient, $\frac{\text{Side force}}{q_\infty S_{ref}}$

C_{N_α} normal-force-curve slope, $\frac{\partial C_N}{\partial \alpha}$, per deg

C_{L_α} lift-curve slope, $\frac{\partial C_L}{\partial \alpha}$, per deg

$C_{m_{C_N}}$ longitudinal stability parameter (referred to body axes), $\frac{\partial C_m}{\partial C_N}$

$C_{m_{C_L}}$ longitudinal stability parameter (referred to stability axes), $\frac{\partial C_m}{\partial C_L}$

C_{l_β} effective-dihedral parameter, $\frac{\Delta C_l}{\Delta \beta}$, per deg

C_{n_β} directional-stability parameter, $\frac{\Delta C_n}{\Delta \beta}$, per deg

C_{Y_β} side-force parameter, $\frac{\Delta C_Y}{\Delta \beta}$, per deg

C_{m_δ} longitudinal-control-effectiveness parameter, $\frac{\Delta C_m}{\Delta \delta_e}$, per deg where $\delta_e = \delta_{e,R} = \delta_{e,L}$

C_{l_δ} lateral-control-effectiveness parameter, $\frac{\Delta C_l}{\Delta \delta_e}$, per deg where $\delta_e = \delta_{e,R} = -\delta_{e,L}$

C_{n_δ} directional-control-effectiveness parameter, $\frac{\Delta C_n}{\Delta \delta_r}$, per deg

L/D lift-drag ratio, $\frac{C_L}{C_D}$

C_p pressure coefficient, $\frac{p - p_\infty}{q_\infty}$

c	local chord, ft
$\bar{c}$	mean aerodynamic chord of exposed basic wing planform, ft
D	body diameter, ft
M	free-stream Mach number
p	static pressure, lb/sq ft
p_∞	free-stream static pressure, lb/sq ft
q_∞	free-stream dynamic pressure, lb/sq ft
S_{ref}	model reference area, $\frac{\pi D^2}{4}$, sq ft
t	local airfoil thickness, ft
α	angle of attack, deg
β	angle of sideslip, deg
$\frac{x_{cg}}{D}$	center-of-gravity location forward of the model base
$\frac{x_{cp}}{D}$	center-of-pressure location forward of the model base
$\delta_{e,R}$	right elevon deflection angle (positive T.E. down), deg
$\delta_{e,L}$	left elevon deflection angle (positive T.E. down), deg
δ_r	rudder deflection angle (positive T.E. left), deg
θ_c	vertical-tail cant angle (positive tip outward), deg
θ_t	vertical-tail toe-in angle, deg

Subscripts:

o	conditions at zero angle of attack or zero lift
max	maximum
b	body base

c balance chamber

r rocket-engine base

MODEL DESCRIPTION

Two vehicle configurations were employed in this investigation: the complete two-stage launch vehicle and the first-stage winged reusable booster. General model arrangements are shown in figure 1 and the details, in figure 2. Photographs of the launch vehicle and first-stage reusable booster are shown in figure 3 and model dimensions are given in table I.

Complete Launch Vehicle

The complete launch vehicle model consisted of two stages in tandem as shown in figure 1. The first stage consisted of a ballistic rocket booster stage with a length-diameter ratio of 3.65 including interstage structure together with a wing and other reusable provisions to be described later, a second-stage expendable booster with a length-diameter ratio of 2.92 including interstage structure, and a representative ogival spacecraft having a length-diameter ratio of 2.21 including interstage structure. Four simulated rocket engines, displaced 45° from the vertical axis of symmetry were mounted parallel to the body axes to simulate the launch arrangement. Two 15° half conical shrouds were employed to provide protection of the two upper rocket engines from aerodynamic loads during launch and the wing-body-juncture fairing was shaped to provide protection for the two lower engines. At the body base a short parabolic boattail fairing was incorporated. (See fig. 2(b).) Details of the shrouds, rocket engines, and spacecraft are given in figures 2(a) and (b).

Winged Reusable Booster

Arrangements of the complete first-stage winged reusable booster are shown in figure 1. Generally it consisted of two assemblies; the complete ballistic rocket booster and the complete winged reusable system attached thereto. For the flyback configuration, the upper stages were removed from the ballistic first stage and a spherical forebody was attached.

A trapezoidal wing (fig. 2(a)) with a 65° leading-edge sweep angle was mounted on the rocket booster so that the center of gravity coincided with 22 percent of the exposed mean aerodynamic chord. The exposed planform area (neglecting trailing-edge extensions) was $7.5D^2$, the taper ratio was 0.35, and 5° of geometric dihedral was employed. The wing was mounted so that the uppermost wing element at the plane of symmetry was tangent to the body diameter - that is, the chord plane was parallel to and $t_{max}/2$ below the body diameter. The basic airfoil section consisted of a symmetrical 10-percent-thick circular

arc with a leading-edge radius of $t_{max}/6$ and a trailing-edge thickness of $t_{max}/3$; no twist or camber was incorporated. To improve subsonic L/D characteristics a trailing-edge extension on the wing amounting to 15 percent of the local chord and consisting of simple wedge profile was installed as shown in figure 2(a). At the center section, inboard of the 10 percent semispan station, a center flap with a straight trailing edge amounting to 15 percent of the local chord at the 10 percent station was provided.

The vertical tails (fig. 2(a)) were located outboard at the wing tips, and employed 15° of outboard cant. Toe-in angles of 0° and 5° were provided by rotating the vertical tail about its midchord. The airfoil section was similar to that for the wing but without the trailing-edge extensions. The taper ratio was 0.60.

Two propulsion engine nacelles are under consideration for this vehicle. One consists of a fully retractable nacelle and the other, a semisubmerged nacelle. At the test Mach numbers the vehicle would be in a supersonic glide and the retractable nacelle was considered to be in the retracted position. Installation of the semisubmerged nacelle is shown in figure 1. Details of the semisubmerged engine nacelle are given in figure 2(b). A simple elliptic cylindrical pod to simulate a crew nacelle was located on the wing leading edge at 20 percent of the left wing semispan. It was mounted with its axis on the wing chord plane. (See figs. 1 and 2(a).)

Control Surfaces

Nearly full-span elevons amounting to 20 percent of the basic chord were provided. They extended from 10 percent to 90 percent of the exposed semispan (not including tip fairing). Deflection angles of 0° and ±20° were provided with hinge plates. The elevons were considered to provide both pitch and roll control.

Directional control was provided by 0.30c control surfaces located on the trailing edge of the vertical tails and extending from approximately the 10 percent station to the tip. By means of hinge plates provisions were made for deflection angles of 0° and -10°.

APPARATUS AND TESTS

The tests were conducted in the Langley Unitary Plan wind tunnel at Mach numbers of 2.36, 2.96, and 4.63, at angles of attack from -4° to 35°, and at angles of sideslip of 0° and 4°. The launch vehicle was tested from angles of attack of -4° to 16° and the first-stage winged reusable booster from -4° to 35°. Test Reynolds number per foot was approximately 3×10^6 for the launch vehicle and 2×10^6 for the reusable booster. For the flyback configuration, longitudinal, lateral, and directional control deflections of -20°, ±20°, and -10°, respectively, were tested.

All experiments were conducted with artificial transition consisting of 1/16-inch-wide strip of No. 60 carborundum grains located on the spherical forebody rearward of the body juncture and at the 0.10c station of both surfaces of the wing and vertical tails.

Six-component static aerodynamic force and moment measurements were obtained by means of an internally mounted strain-gage balance. Angles of attack and sideslip were corrected for balance and sting deflection under load. All drag data are presented with no base-pressure corrections applied; however, pressure measurements were made in the balance chamber, on the body base, and on the rocket engines. All forces and moments are reduced to coefficient form and are referred to the area of the body base and its diameter. The moment reference station was located 0.90 diameter forward of the model base. (See fig. 1.)

RESULTS AND DISCUSSION

The results of this investigation have been divided into two primary parts. The first consists of the data for the complete launch vehicle; the second, the data for the first-stage winged reusable booster. Figures 4 to 8 present the basic and summary aerodynamic characteristics of the complete launch configuration. Figures 9 to 18 include the basic and summary data for the first-stage winged reusable booster. All force and moment data are referred to the area of the body base and its diameter. All moments are referred to the assumed center of gravity which was 0.90 diameter forward of the model base, which is the estimated center of gravity for the first stage during flyback to the recovery site.

Complete Launch Vehicle

For the complete launch vehicle, the normal-force-curve slope decreased and became progressively nonlinear with increasing Mach number. (See figs. 4 and 5.) The launch vehicle is shown in figures 4 and 5 to be longitudinally unstable about the chosen moment reference center and became progressively more unstable with increasing Mach number. In order to assess the longitudinal stability adequately, consideration must be given to the actual center of gravity and its change during launch as the fuel is progressively consumed. An estimate of the center of gravity at the representative test Mach numbers is shown in figure 8. The variation of center of gravity shown with Mach number is obtained by taking into account the propellant burned over a representative launch trajectory for this vehicle. From figure 8 it is concluded that the launch vehicle's longitudinal center of pressure is rearward of the estimated center of gravity for all test Mach numbers at an angle of attack of 0°.

Figure 7 shows the launch vehicle to be directionally unstable at angles of attack of 0° and 12° about the chosen moment reference center. From figure 8 it is concluded that the lateral center of pressure is rearward of the estimated center of gravity for all test Mach numbers at an angle of attack of 0°.

Longitudinal stability.- Figure 9(a) shows that for the first-stage reusable booster the pitching-moment-coefficient curves were nonlinear and were characterized by a large range of lift coefficients with nominal stability for the angle-of-attack and Mach number range of the tests. The level of the pitching-moment-coefficient curves increased with Mach number and may require both positive and negative control deflections to trim the vehicle. Installation of the vertical tails shows significant improvements in stability throughout the Mach number range. It seems apparent that the usual end-plate effect has been achieved which accounts for the improvement in longitudinal stability. Toeing-in the vertical tails 5° resulted in a decrease in the level of the pitching-moment curves and was probably caused by increased wing-tip loading. Installation of the semisubmerged engine nacelle provided an increase in pitching-moment level in the low angle-of-attack range but generally resulted in a more severe stable break in the pitching-moment curves in the high angle-of-attack range. This was probably caused by high positive pressures on the forward facing ramp, employed to close the inlets and protect the engines, as the angle of attack was increased positively.

At these test Mach numbers the first-stage winged reusable booster would be expected to be in a supersonic glide attitude and the region of main interest is near maximum L/D conditions. Figure 10 summarizes the longitudinal stability near maximum L/D. All the results for the vertical tails on indicate positive longitudinal stability, and for the vertical tails toed-in 5° the highest stability over the test Mach number range is indicated.

Drag and lift-drag-ratio characteristics.- The drag coefficients at 0° angle of attack are shown in figure 10. Addition of the vertical tails resulted in an increase in $C_{D,o}$ of about 20 percent over the Mach number range. This large increase in drag probably resulted from interference drag at the wing and tail juncture and improper alinement with the local flow. Figures 9(a) and 10 indicate that the vertical tails generally reduced the drag due to lift as a probable result of the end-plate effect on lift distribution. Toeing in the vertical tails 5° decreased $C_{D,o}$ at the lower Mach number (fig. 10). This decrease was probably caused by closer alinement with the local flow direction and the resultant reduction of drag due to side force on the vertical tail. The maximum value of L/D for the 5° toe-in configuration varied from about 1.9 to 1.45 over the Mach number range. Installation of the semisubmerged engine nacelle degraded the drag at lifting conditions as shown in figure 9(a) due to the increased pressure on the forward facing inlet closure ramp.

Lateral-directional stability.- Positive effective dihedral (fig. 11) is shown above angles of attack of 14° at a Mach number of 2.36 and 8° at a Mach number of 4.63 for all configurations tested. The favorable influence of angle of attack of a highly swept wing on effective dihedral is illustrated by the results shown for 0° and 20°. (See fig. 12.)

The substantial contribution to directional stability of the outboard mounted vertical tails is shown in figure 12. Employing 5° of toe-in of the vertical tails resulted in an increase in directional stability about equal to

the installation of the vertical tails themselves. Surprisingly little effect of angle of attack up to about 35° on yawing-moment coefficient is shown for all configurations tested (fig. 11). The stability level shows very little deterioration with increasing supersonic Mach number. Figure 12 also shows the small adverse effect on directional stability of the semisubmerged flyback engine nacelle which was located appreciably forward of the center of gravity. (See fig. 1.)

Control effectiveness.- Comparison of figures 9(a) and 13(a) shows that an up-elevon deflection of 20° caused a severe decrease in longitudinal stability at all Mach numbers which resulted in unstable characteristics at all lift coefficients greater than about 3.0. This deflection resulted in small increases in directional stability (fig. 15). Figure 14 shows the longitudinal instability at conditions near $(L/D)_{max}$ of an up-elevon deflection of 20°. Longitudinal control effectiveness (fig. 18) decreased rapidly with increasing Mach number but increased with angle of attack.

Figure 17 summarizes the lateral directional stability characteristics with deflected lateral and directional controls. Deflection of both rudders to the right 10° or differential elevons ±20° caused generally small effects on C_{l_β} or C_{n_β}. Figure 18 shows that rudder effectiveness decreased with increasing Mach number and angle of attack.

The ability of the differential elevons deflected ±20° to produce roll control is shown in figure 18. The effectiveness increased with angle of attack but decreased with Mach number; however, the Mach number deterioration was considerably reduced at the higher angles of attack. The interaction of roll control on yawing moment can be seen in figures 11(c) and 16(b). An unfavorable yawing moment was introduced which may decrease directional control. From figure 17 it can be seen that there was a positive contribution to directional stability at $\alpha = 20°$ due to differential elevon deflection. These effects would have to be evaluated critically to determine if an adverse effect on dynamic stability would result.

CONCLUDING REMARKS

An investigation has been conducted in the Langley Unitary Plan wind tunnel to determine the longitudinal and lateral-directional stability of a complete launch vehicle and its fixed-wing reusable first stage. In addition, control effectiveness was obtained for the reusable first stage. Test data were obtained at Mach numbers of 2.36, 2.96, and 4.63, angles of attack from -4° to 35°, and sideslip angles of 0° and 4°. Test Reynolds number per foot varied from approximately 2×10^6 to 3×10^6. The principal results may be summarized as follows:

1. The longitudinal and lateral center of pressure of the launch vehicle was rearward of the estimated center of gravity for all test Mach numbers at an angle of attack of 0°.

2. The complete first-stage flyback booster was longitudinally stable throughout the Mach number range, although large changes in stability occurred with angle of attack.

3. Vertical-tail toe-in has been shown to be a powerful tool in improving directional stability. Negligible changes in directional stability with Mach number or angle of attack up to 35° were observed.

4. Severe degradation of longitudinal stability resulted from upward elevon deflections at all test Mach numbers. Longitudinal control effectiveness decreased rapidly with increasing Mach number but increased with angle of attack.

5. Rudder effectiveness decreased with increasing Mach number and angle of attack but deflecting the rudders had little effect on directional or lateral stability.

6. Differential roll-control effectiveness increased with angle of attack but decreased with Mach number.

Langley Research Center,
National Aeronautics and Space Administration,
Langley Station, Hampton, Va., February 4, 1965.

REFERENCE

1. Pierpont, P. Kenneth: Aerodynamic Investigation of a Large Winged Vertical-Take-Off Reusable Orbital Launch Vehicle at Mach 0.4 to 2.1. NASA TM X-996, 1964.

TABLE I.- GEOMETRIC CHARACTERISTICS

[All linear dimensions are in inches]

Reusable first-stage booster -	
Body:	
Length, overall	13.14
Diameter	3.17
Base area	7.88
Length/Diameter, cylindrical body	3.65
Moment reference from base	2.85
Shrouds:	
Length, 15°	2.52
Wing:	
Total area, including trailing-edge extension	122.60
Exposed area, including trailing-edge extension	88.00
Exposed area, neglecting trailing-edge extension	75.40
Root chord at fuselage juncture	9.38
Tip chord	3.28
Span (total)	15.05
Leading-edge sweep, deg	65
Positive dihedral, deg	5
$(t/c)_{max}$	0.10
Leading-edge radius	$t_{max}/6$
Trailing-edge thickness	$t_{max}/3$
Airfoil section	Circular arc
$\bar{c}$, based on exposed area	6.83
Moment reference, from leading-edge wing	$0.22\bar{c}$
Moment reference, distance from body base	2.85
Aspect ratio	1.93
Vertical tail:	
Area, each	9.43
Root, chord	3.65
Tip chord	2.19
Height	3.23
Leading-edge sweep, deg	30
$(t/c)_{max}$	0.10
Leading-edge radius	$t_{max}/6$
Trailing-edge thickness	$t_{max}/3$
Airfoil section	Circular arc
Toe-in, deg	0 and 5
Cant, deg	15
Tail moment arm, c.g. to $(\bar{c}/4)$ tail	7.51
Second-stage expendable rocket booster -	
Length	9.25
Diameter	3.17
Length/Diameter	2.92
Spacecraft -	
Length	7
Diameter, base	3.17

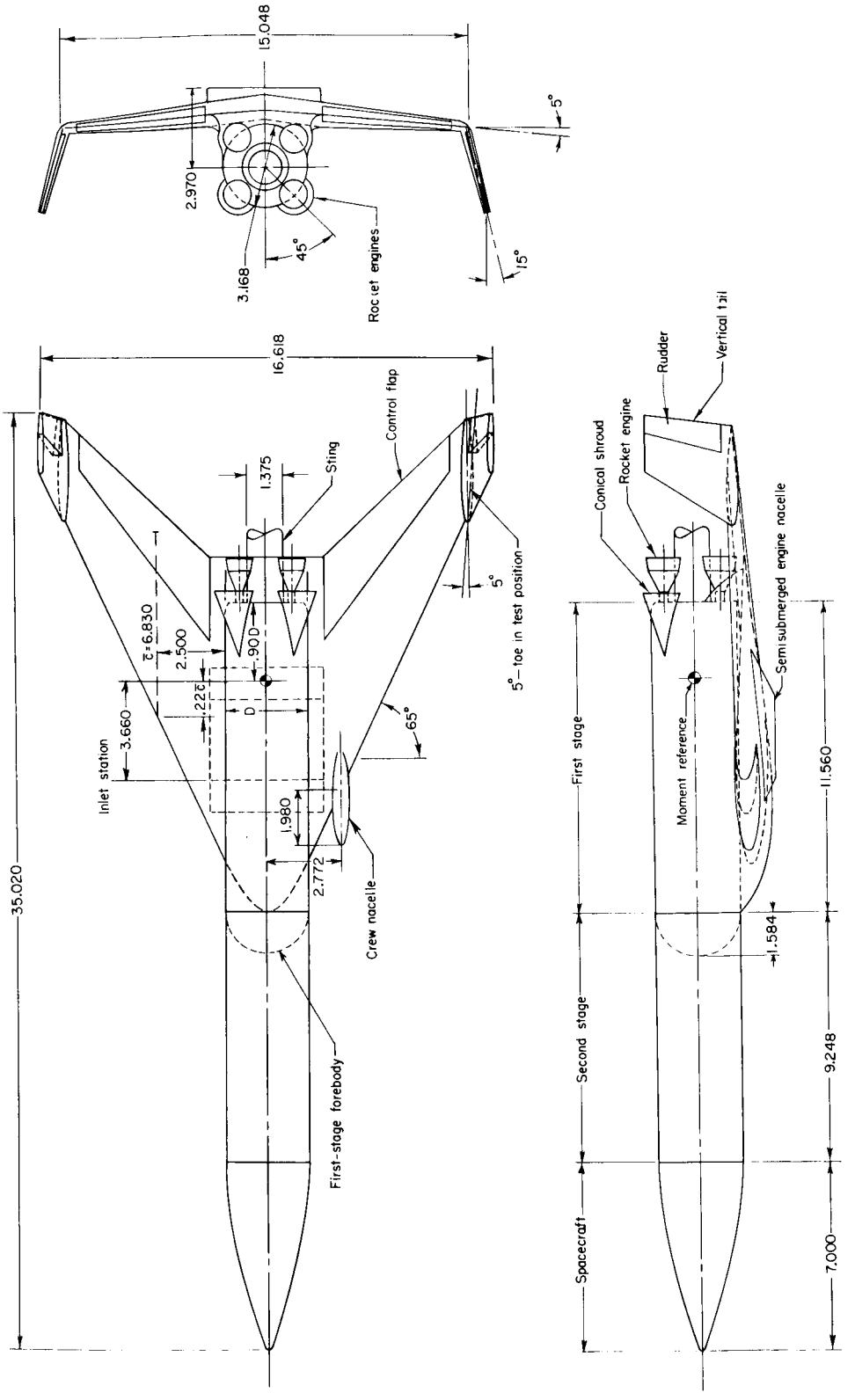

Figure 1.- Arrangement and geometric details of launch vehicle with first-stage reusable booster. All dimensions are in inches unless otherwise noted.

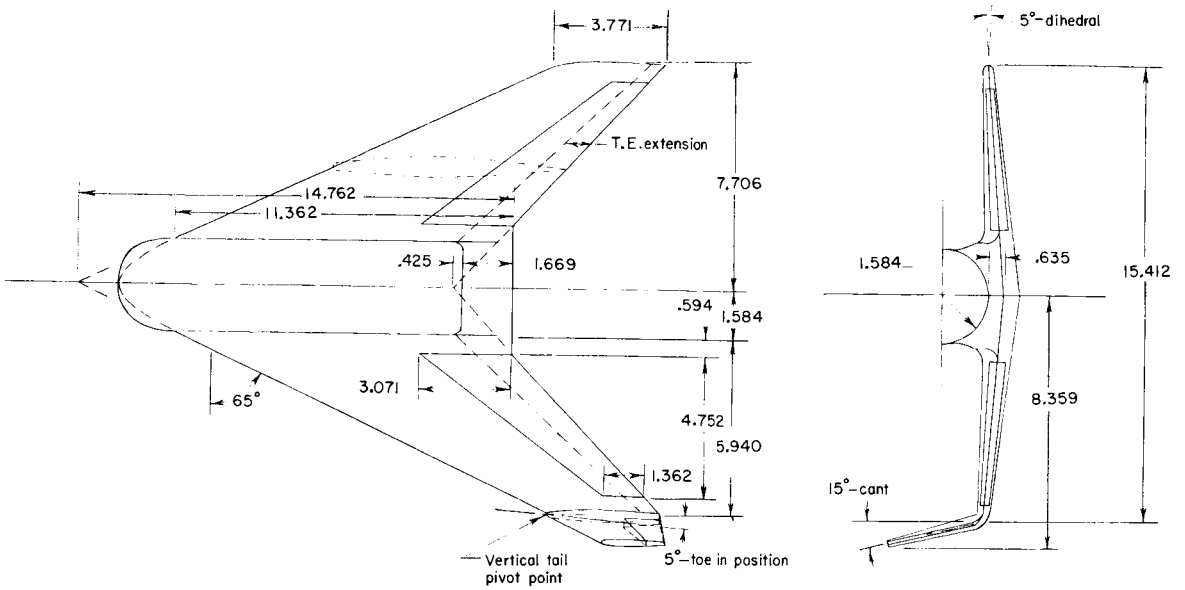

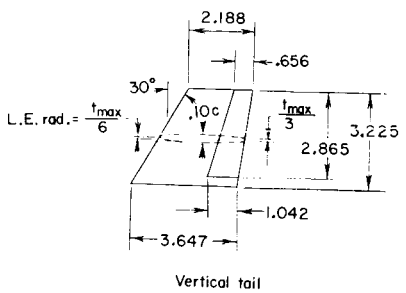

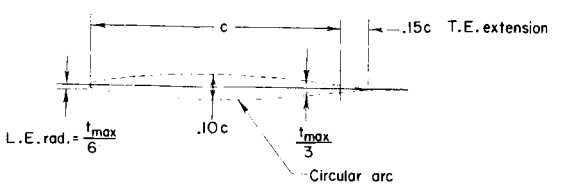

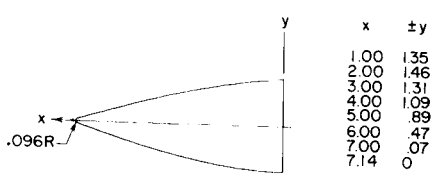

x	±y
1.00	1.35
2.00	1.46
3.00	1.31
4.00	1.09
5.00	.89
6.00	.47
7.00	.07
7.14	0

Spacecraft

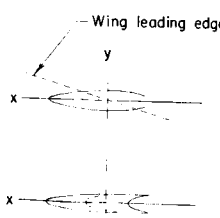

±y	x
0	0.329
.25	.327
.50	.318
.75	.308
1.00	.283
1.25	.255
1.50	.214
1.75	.153
1.85	.116
1.90	.092
1.95	.057
1.98	0

Crew nacelle

(a) Wing, vertical tail, crew nacelle, and payload.

Figure 2.- Details of model components. All dimensions are in inches unless otherwise noted.

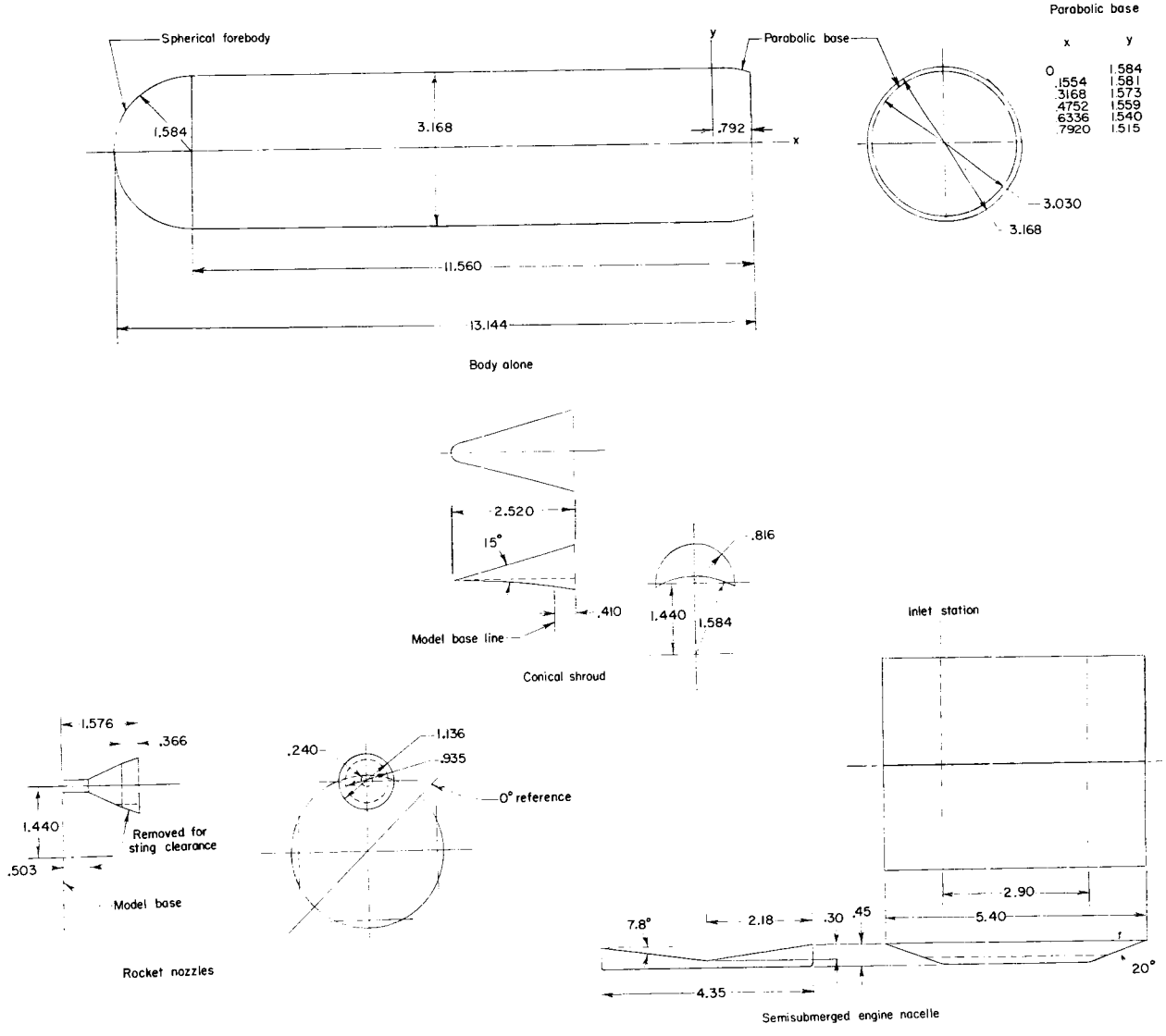

(b) Body alone, conical shrouds, forebody and base arrangement, rocket nozzles, and flyback engine nacelle.

Figure 2.- Concluded.

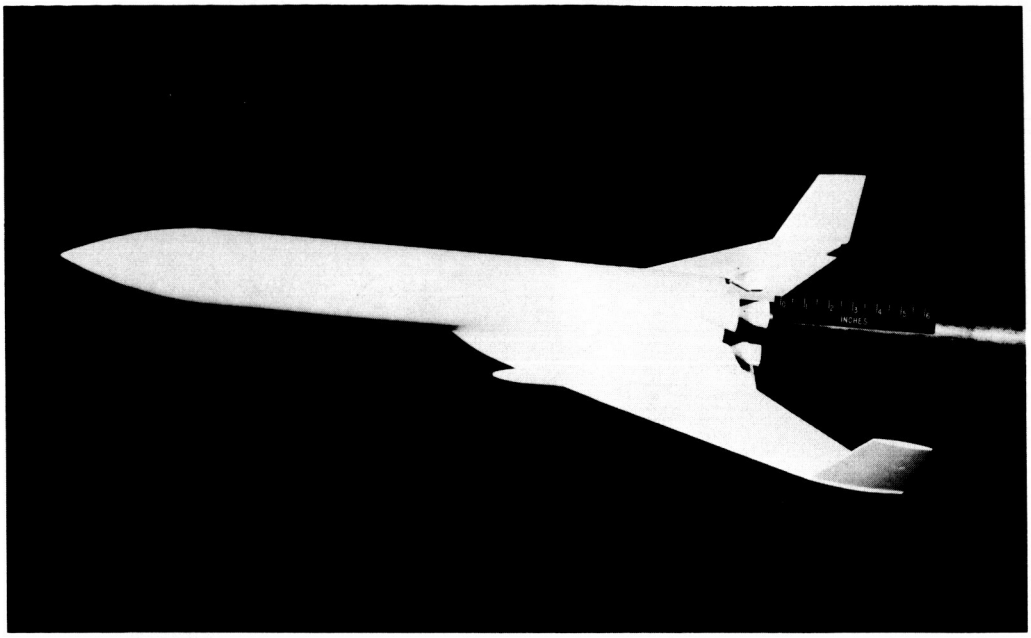

(a) Complete launch configuration. L-64-7561

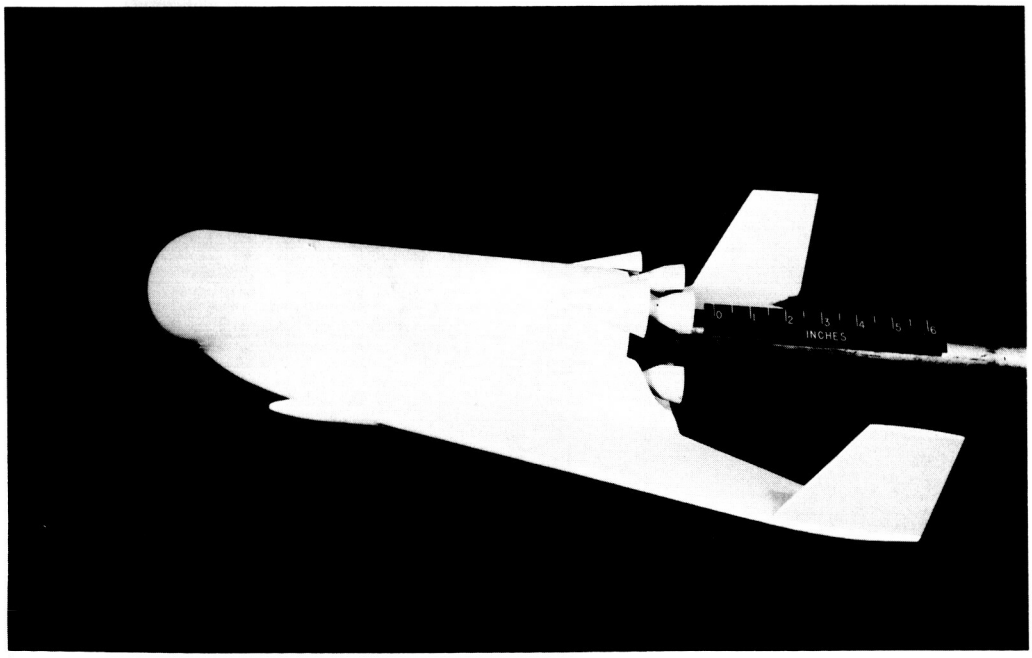

(b) First-stage reusable booster. L-64-7564

Figure 3.- Photographs of models used in investigation.

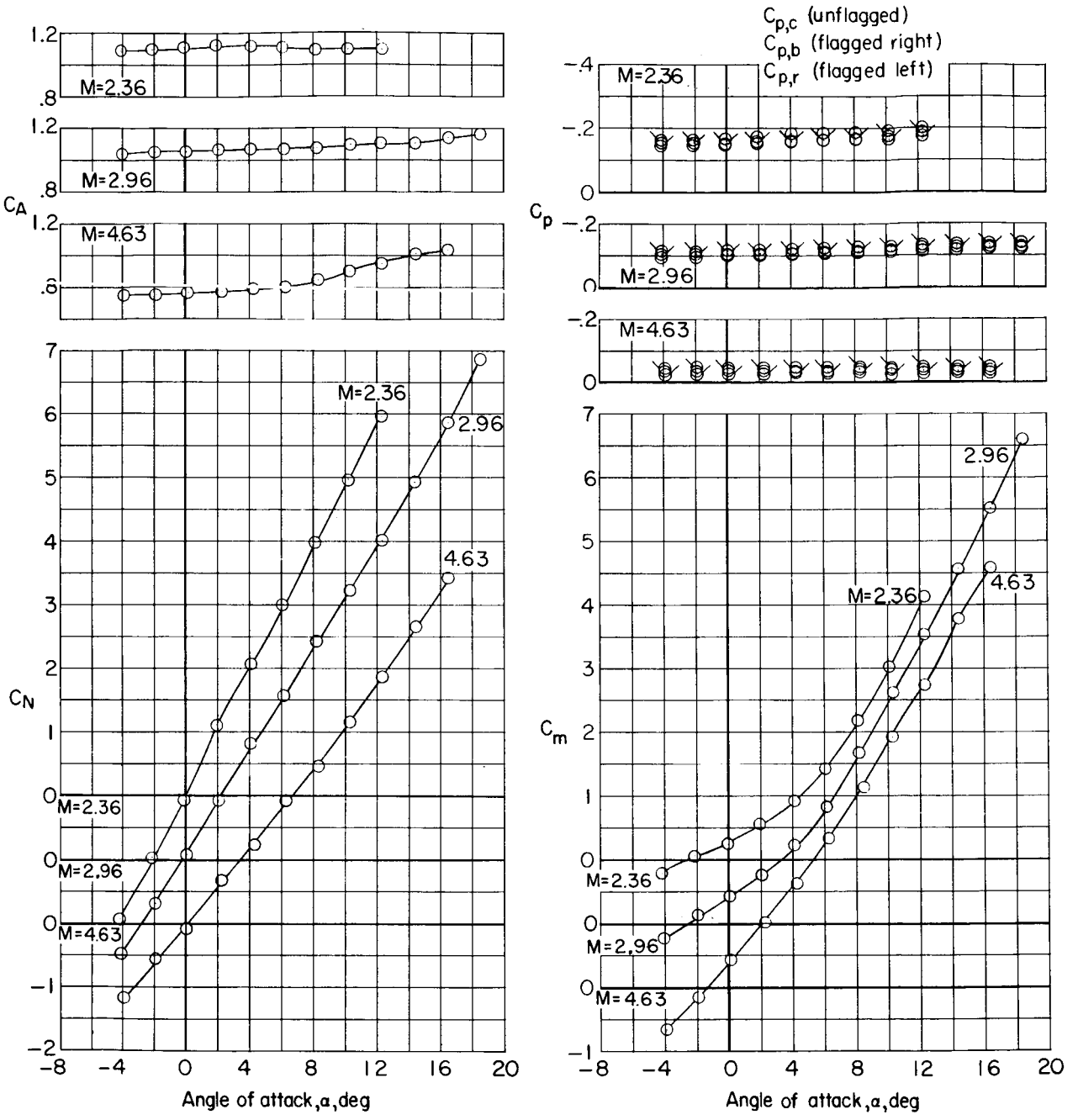

Figure 4.- Longitudinal aerodynamic characteristics of complete launch vehicle. Engine nacelle off; $\theta_t = 5^\circ$; $\theta_c = 15^\circ$; $\beta = 0^\circ$.

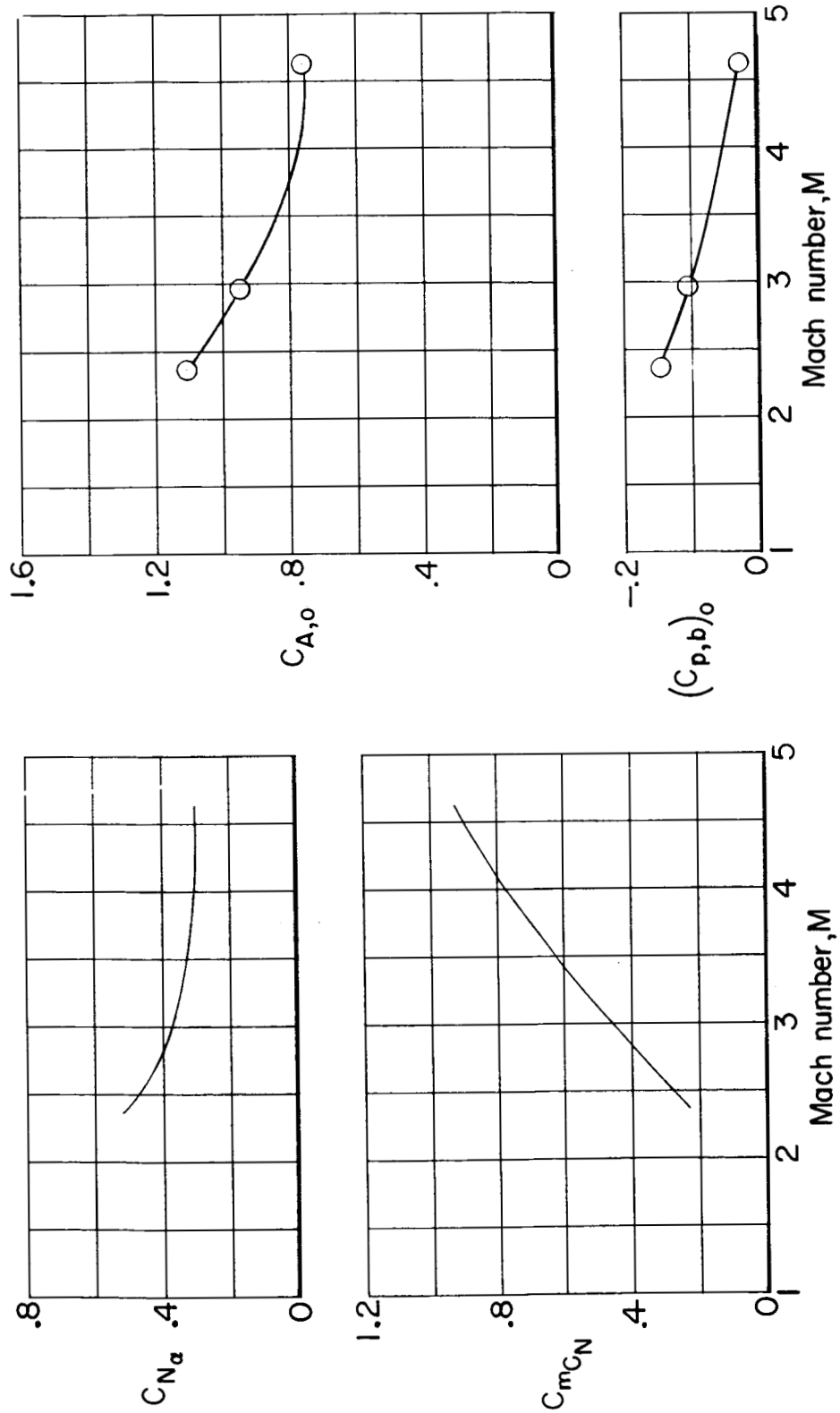

Figure 5.- Variation with Mach number of longitudinal-stability and drag parameters for complete launch vehicle. Engine nacelle off; $\theta_t = 5^o$; $\theta_c = 15^o$; $\beta = 0^o$.

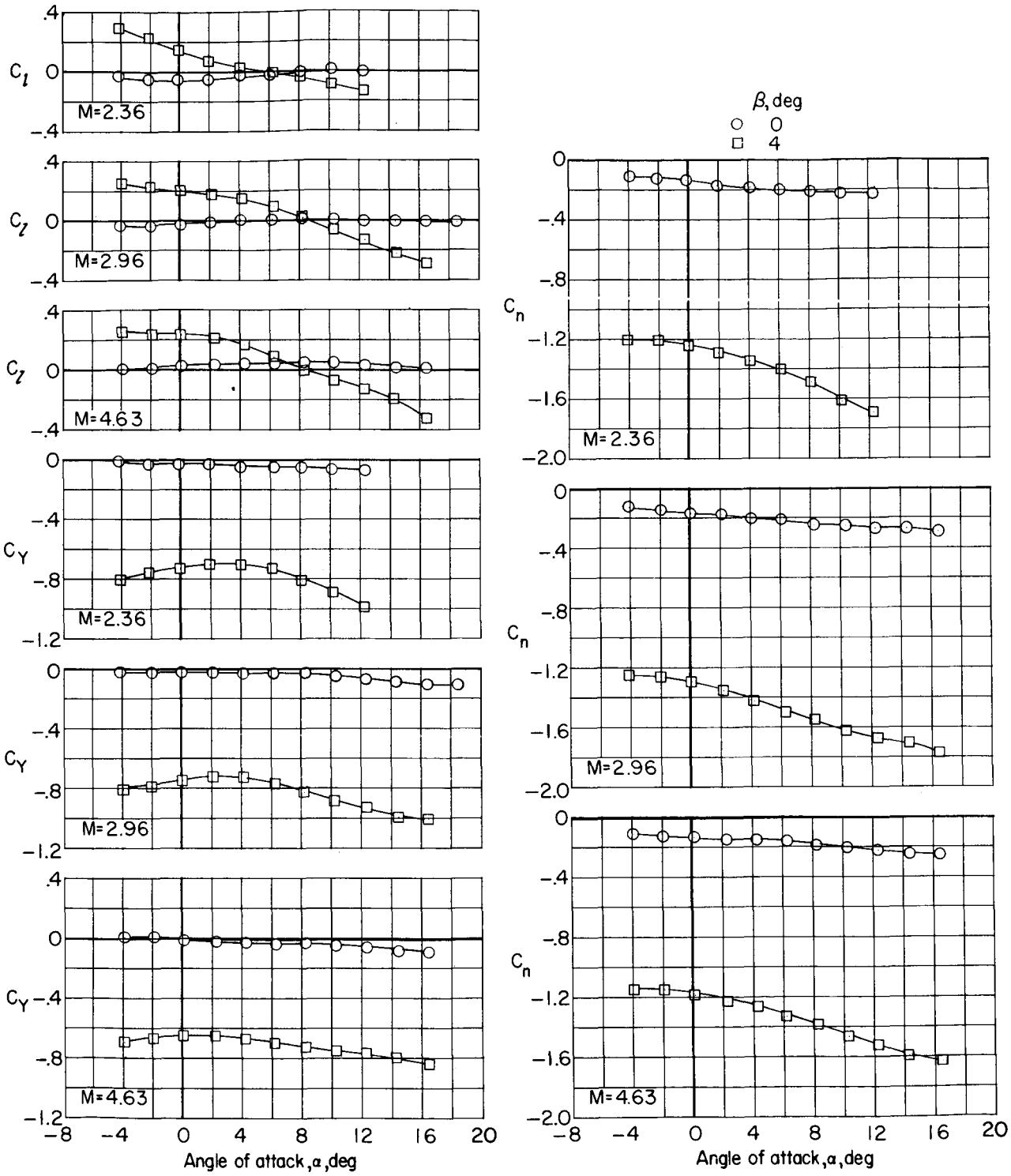

Figure 6.- Lateral aerodynamic characteristics of complete launch vehicle. Engine nacelle off; $\theta_t = 5^\circ$; $\theta_c = 15^\circ$.

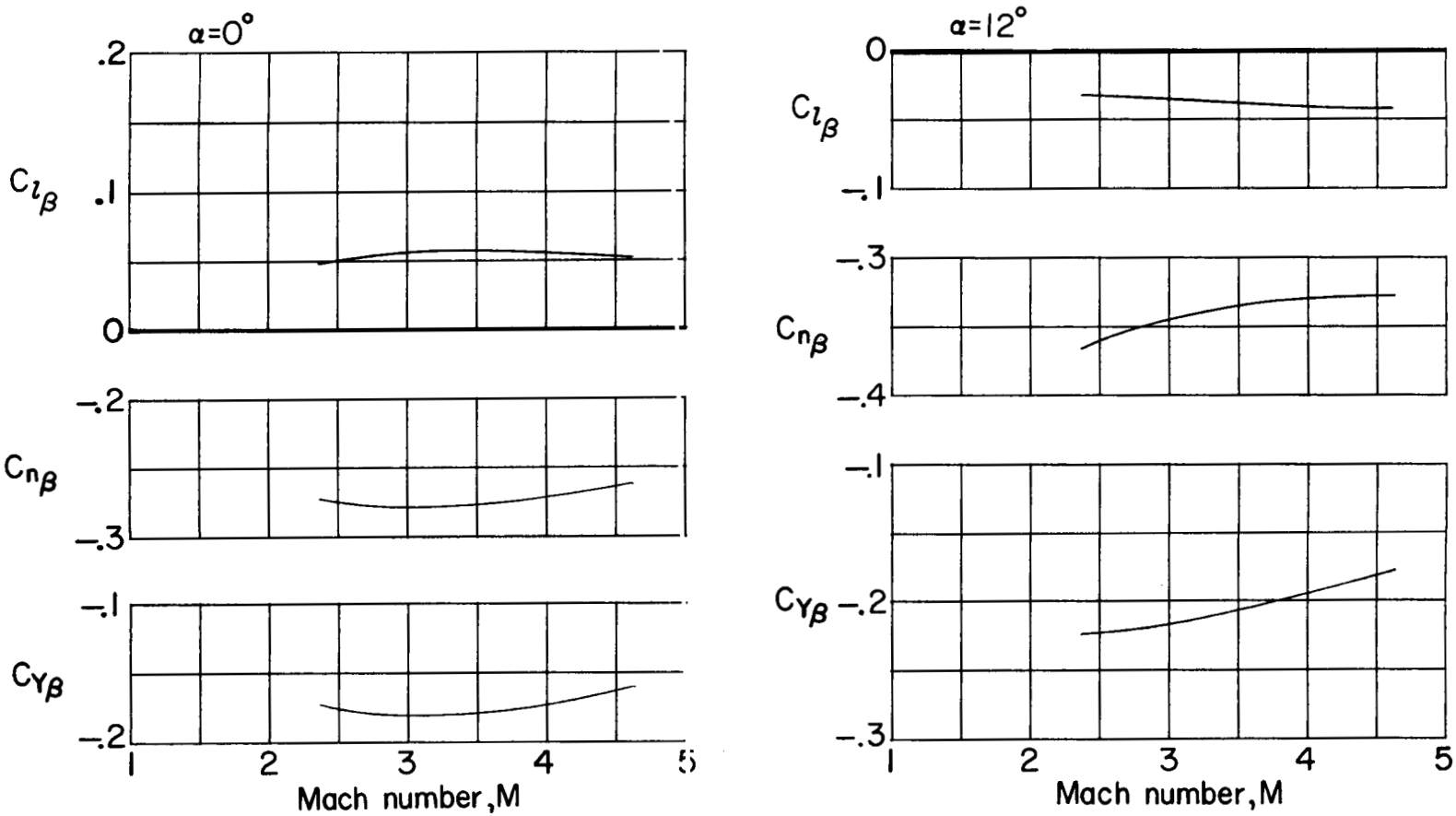

Figure 7.- Variation with Mach number of lateral-directional-stability parameters for complete launch vehicle. Engine nacelle off; $\theta_t = 5^\circ$; $\theta_c = 15^\circ$.

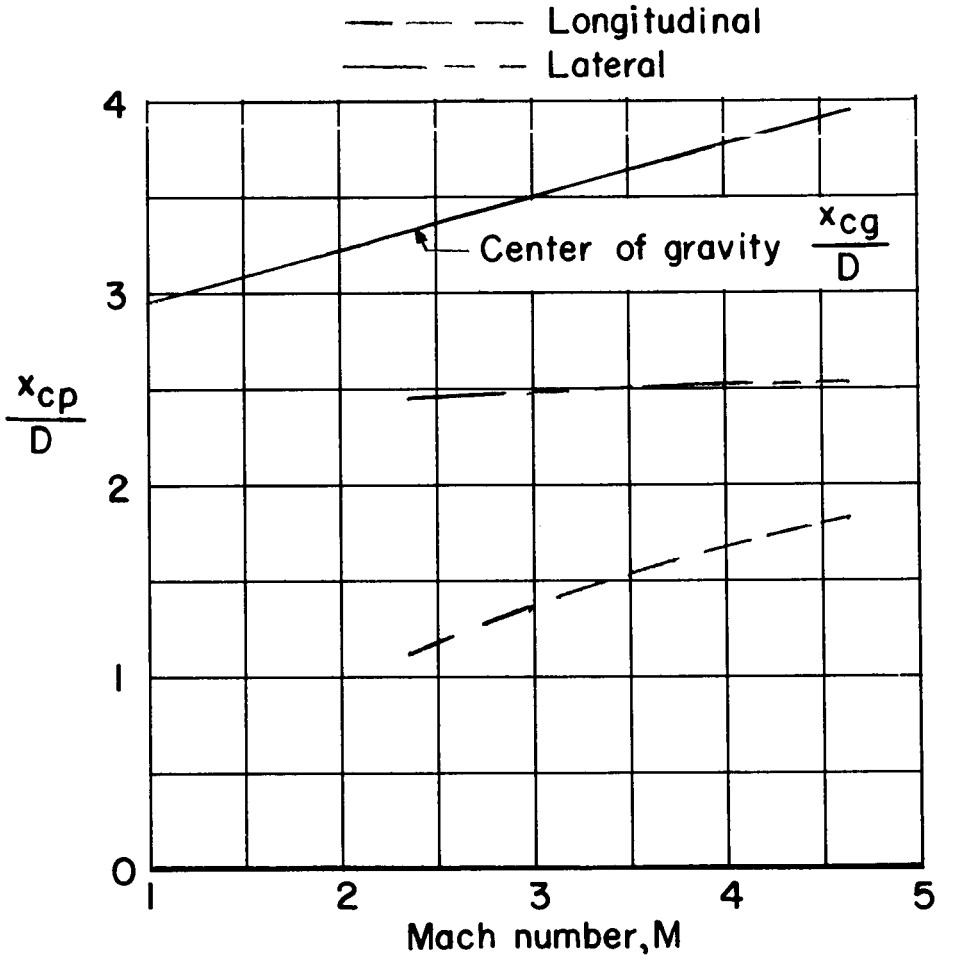

Figure 8.- Comparison of longitudinal and lateral center of pressure for complete launch vehicle compared with estimated flight center-of-gravity location. $\alpha = 0^{\circ}$.

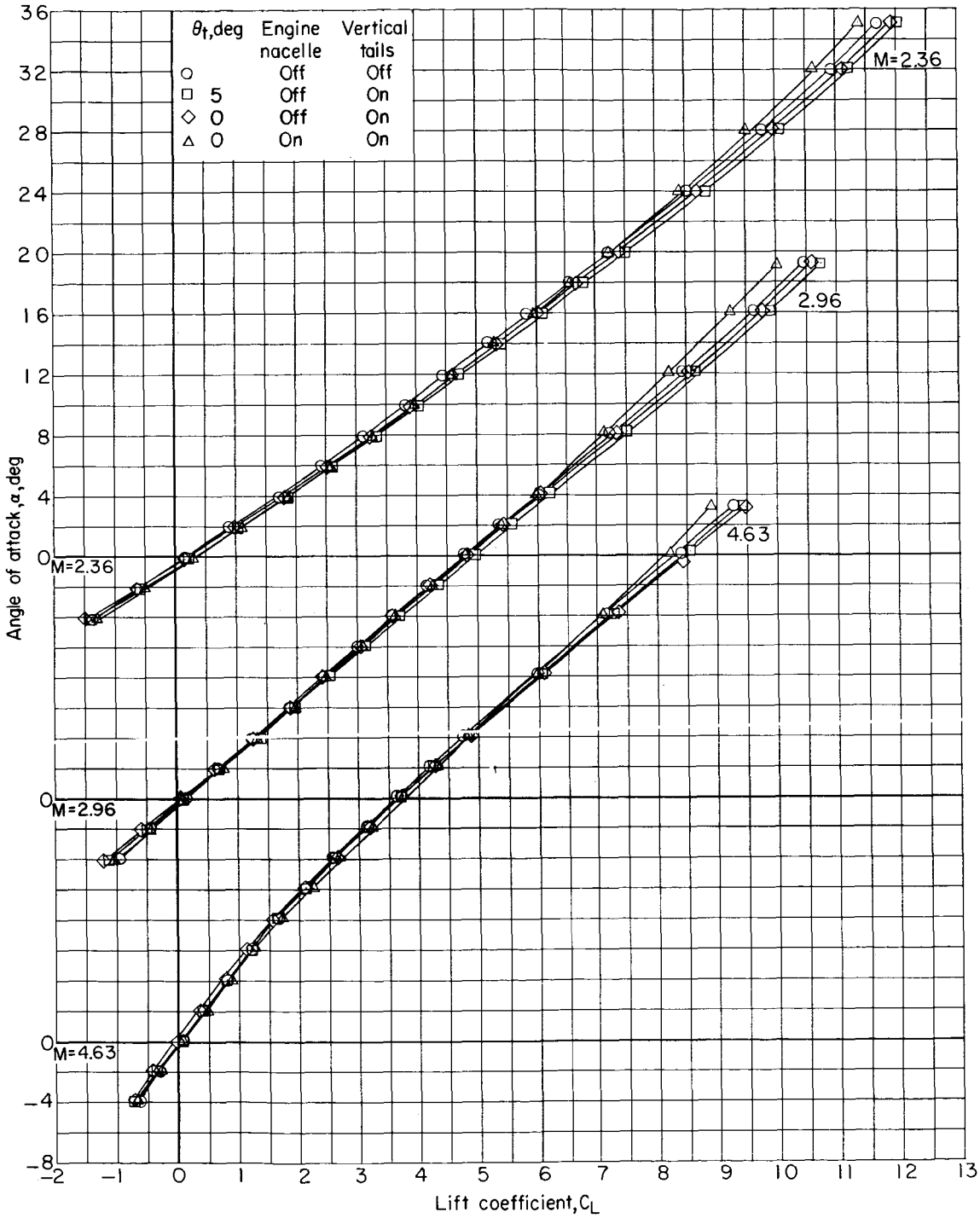

(a) Longitudinal characteristics.

Figure 9.- Longitudinal aerodynamic characteristics of first-stage reusable booster. $\theta_c = 15^o$; $\beta = 0^o$.

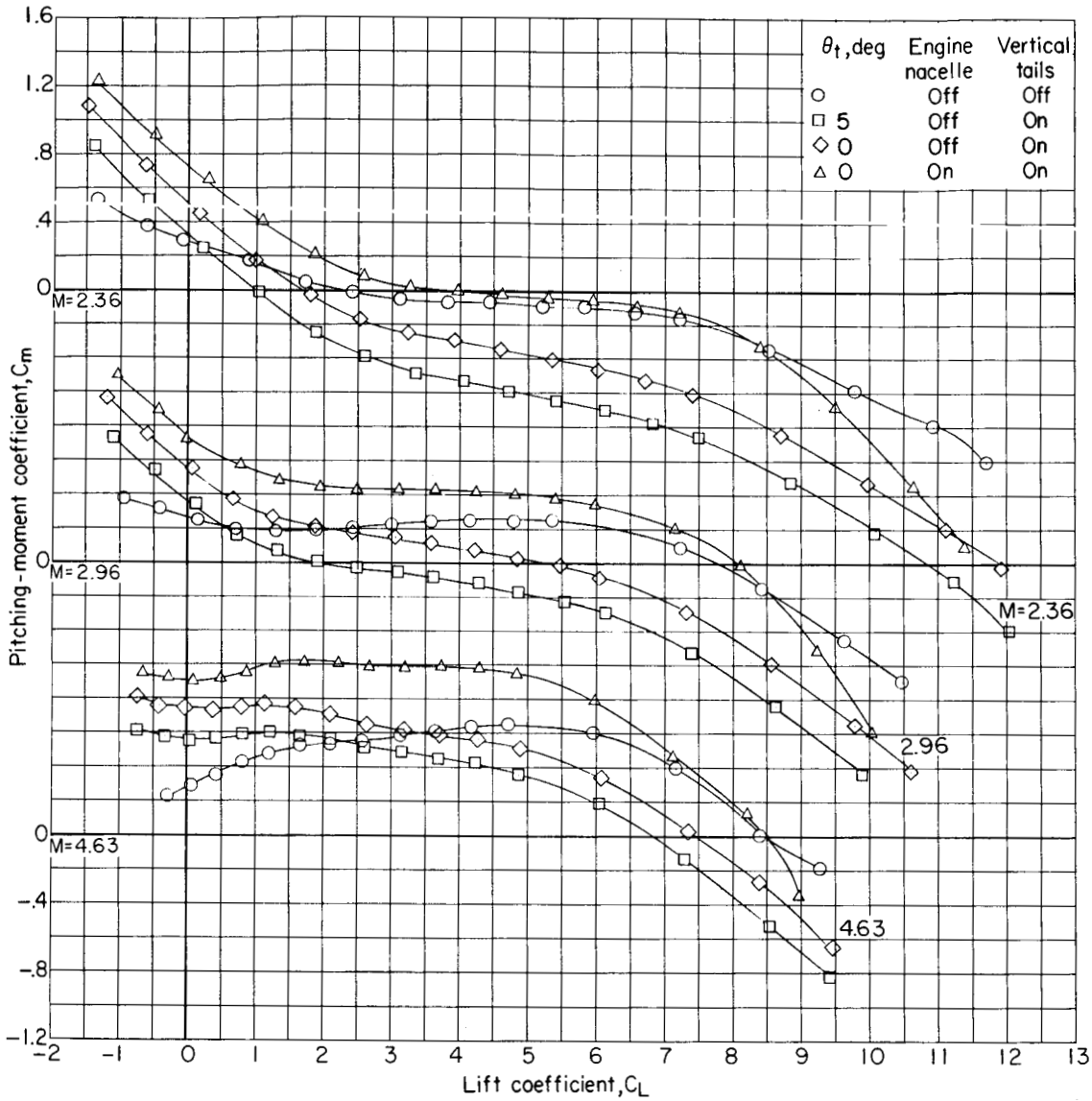

(a) Longitudinal characteristics. Continued.

Figure 9.- Continued.

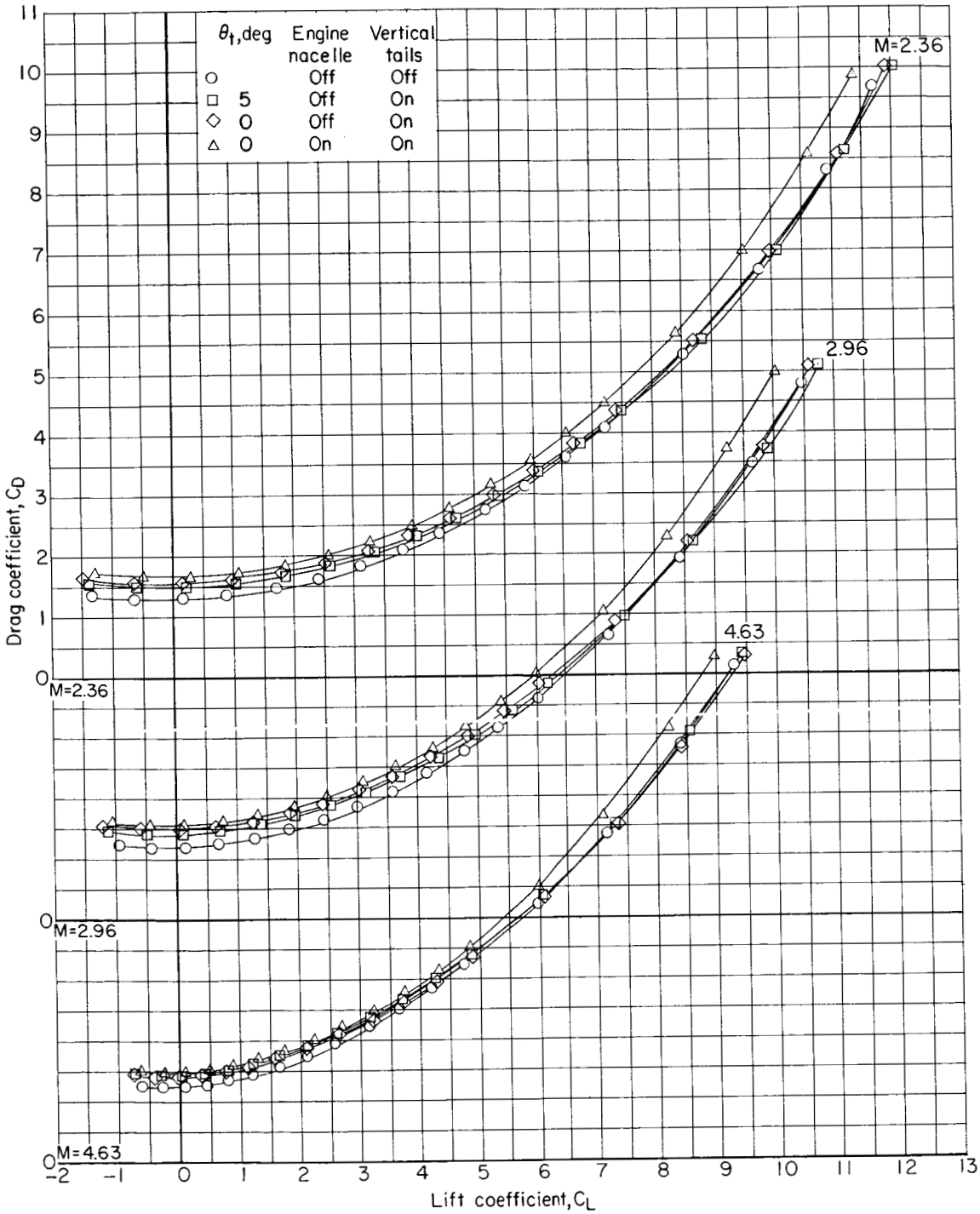

(a) Longitudinal characteristics. Concluded.

Figure 9.- Continued.

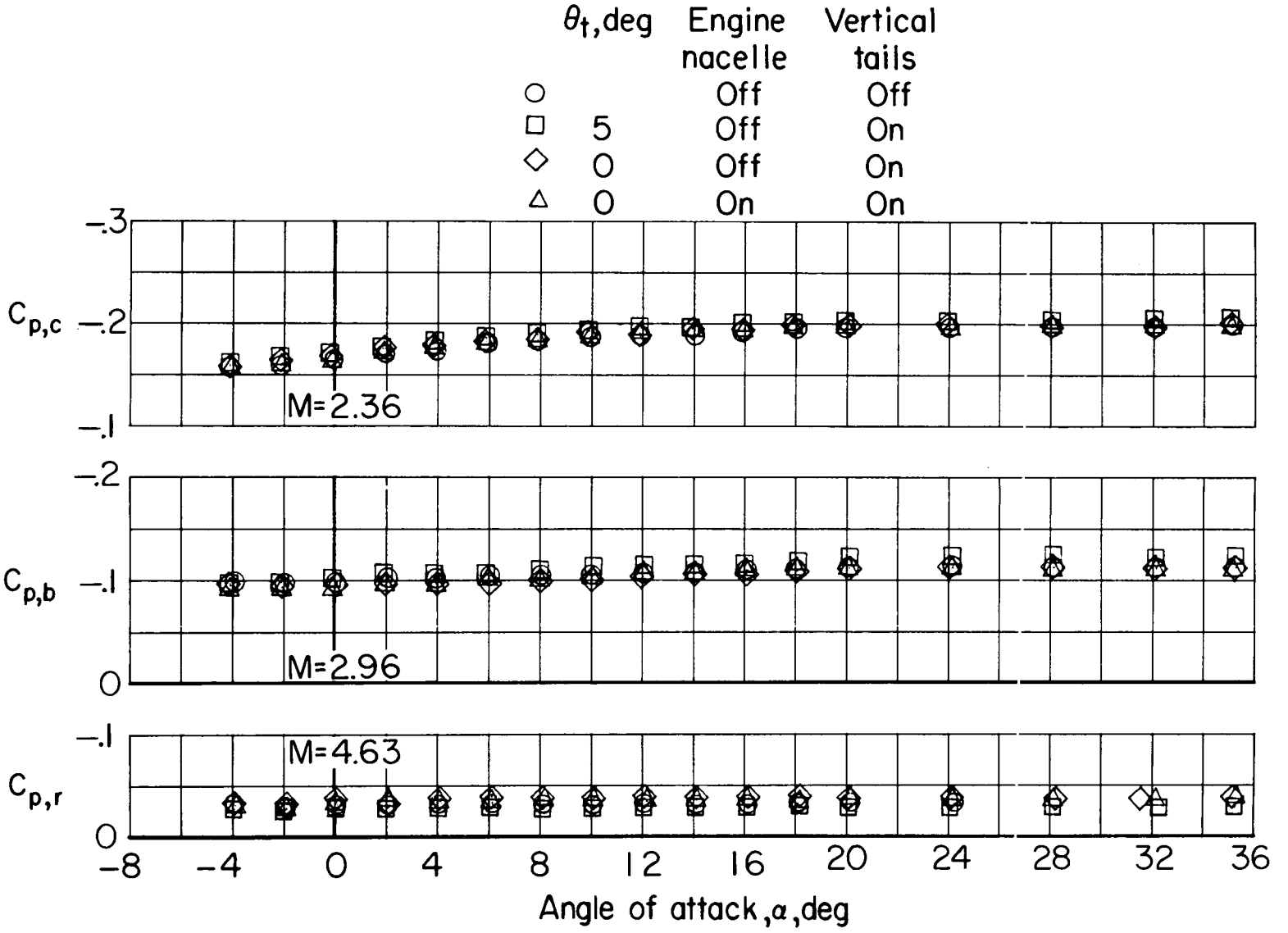

(b) Pressure coefficients.

Figure 9.- Concluded.

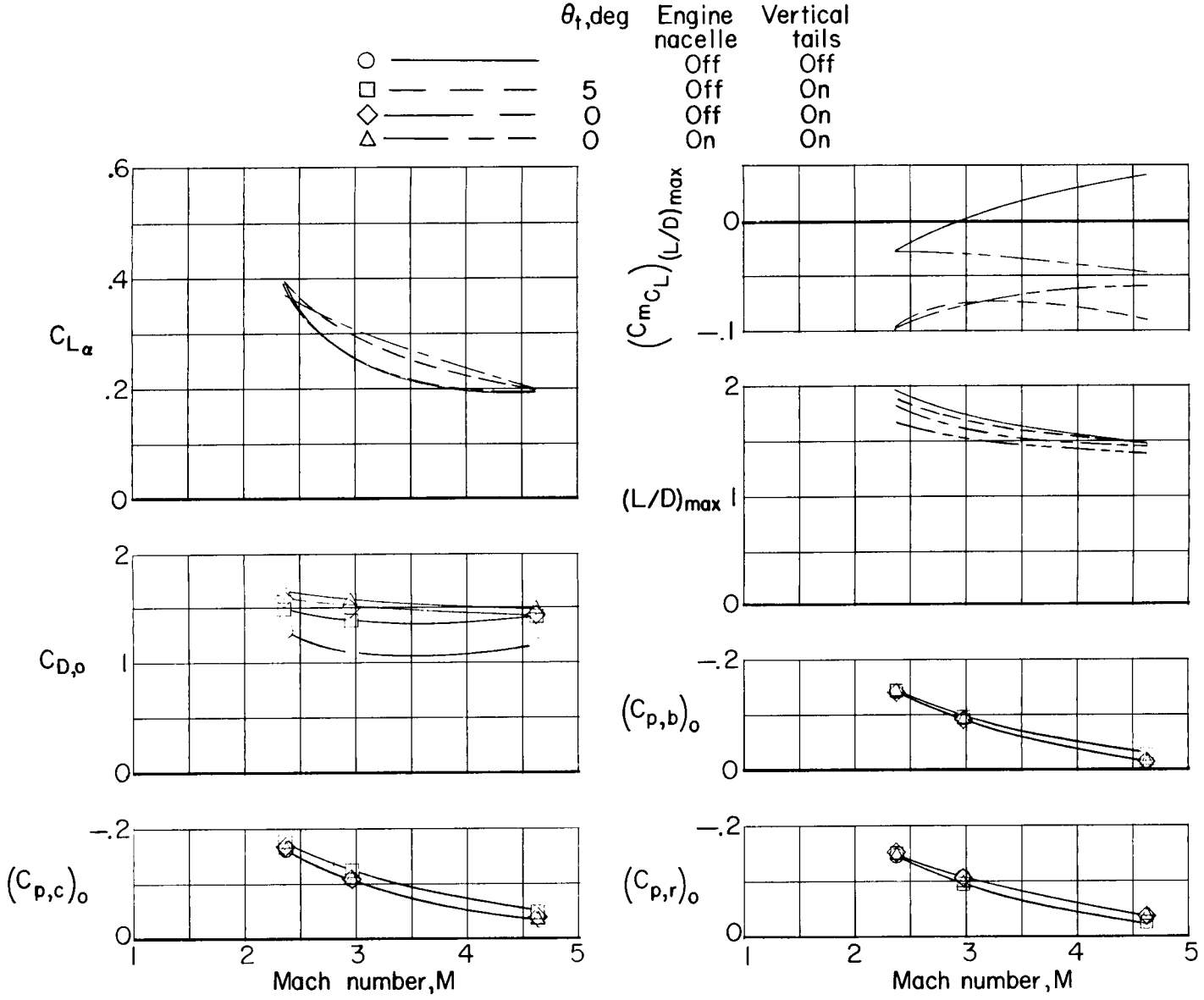

Figure 10.- Variation with Mach number of longitudinal-stability and drag parameters for first-stage reusable booster. $\theta_c = 15^\circ$; $\beta = 0^\circ$.

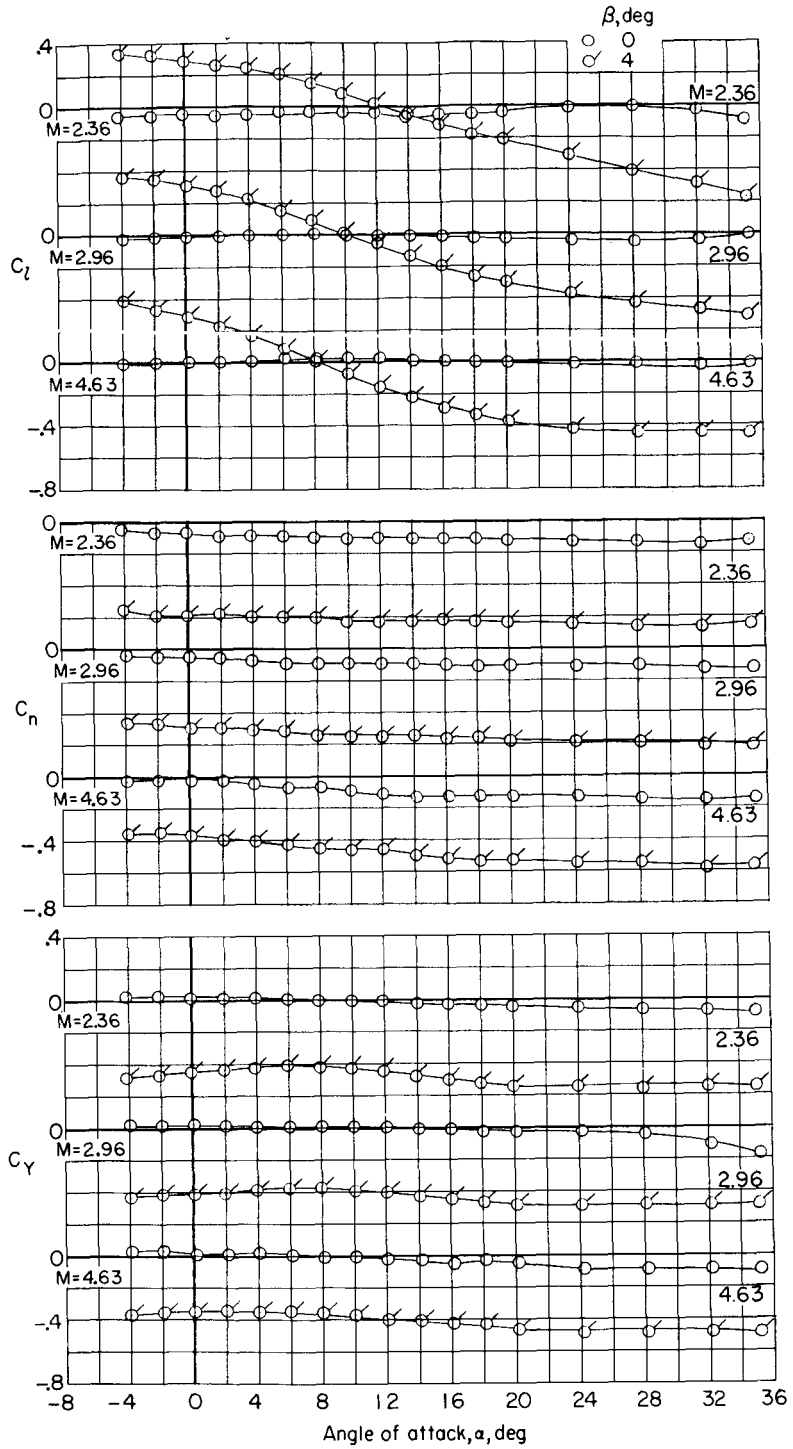

(a) Nacelle and vertical tails off.

Figure 11.- Lateral aerodynamic characteristics of first-stage reusable booster. $\theta_c = 15^\circ$.

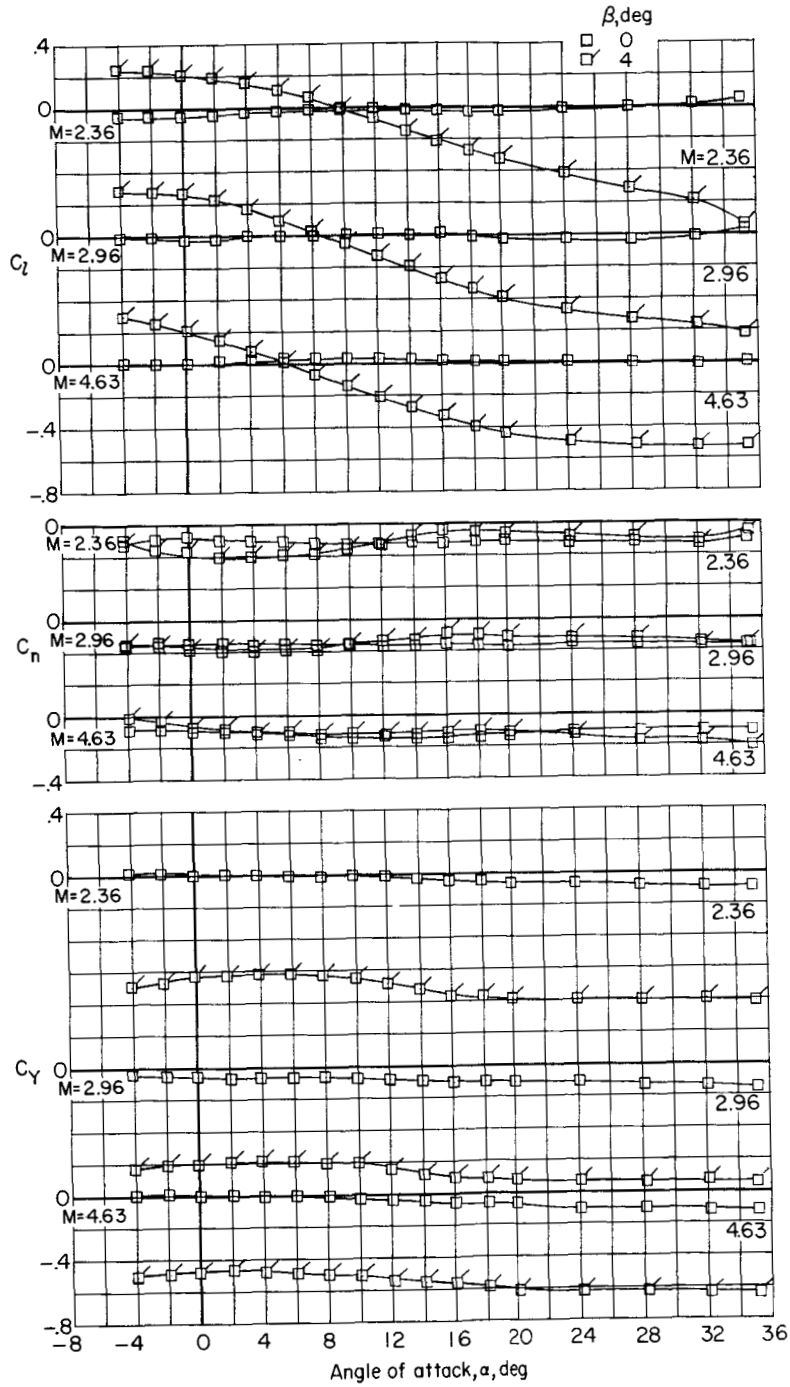

(b) Nacelle off; vertical tails on; $\theta_t = 5^\circ$.

Figure 11.- Continued.

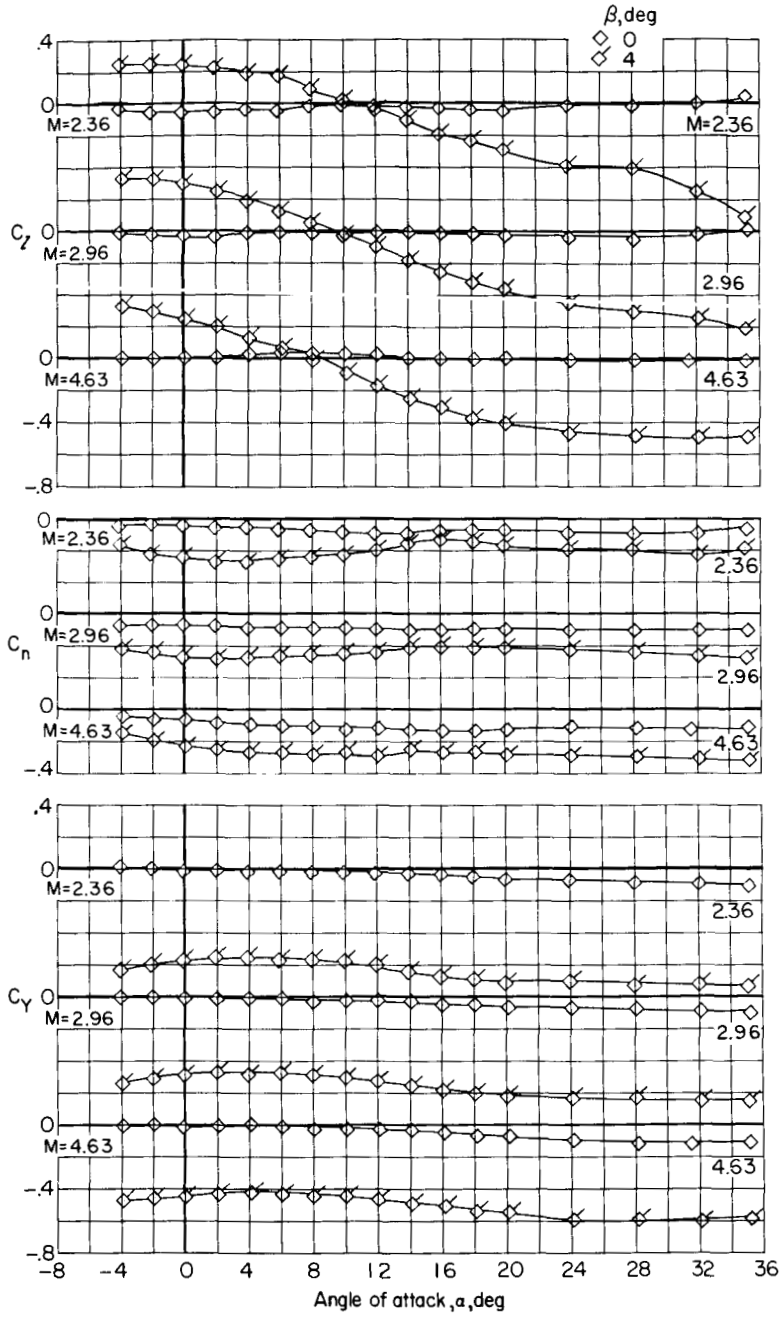

(c) Nacelle off; vertical tails on; $\theta_t = 0^\circ$.

Figure 11.- Continued.

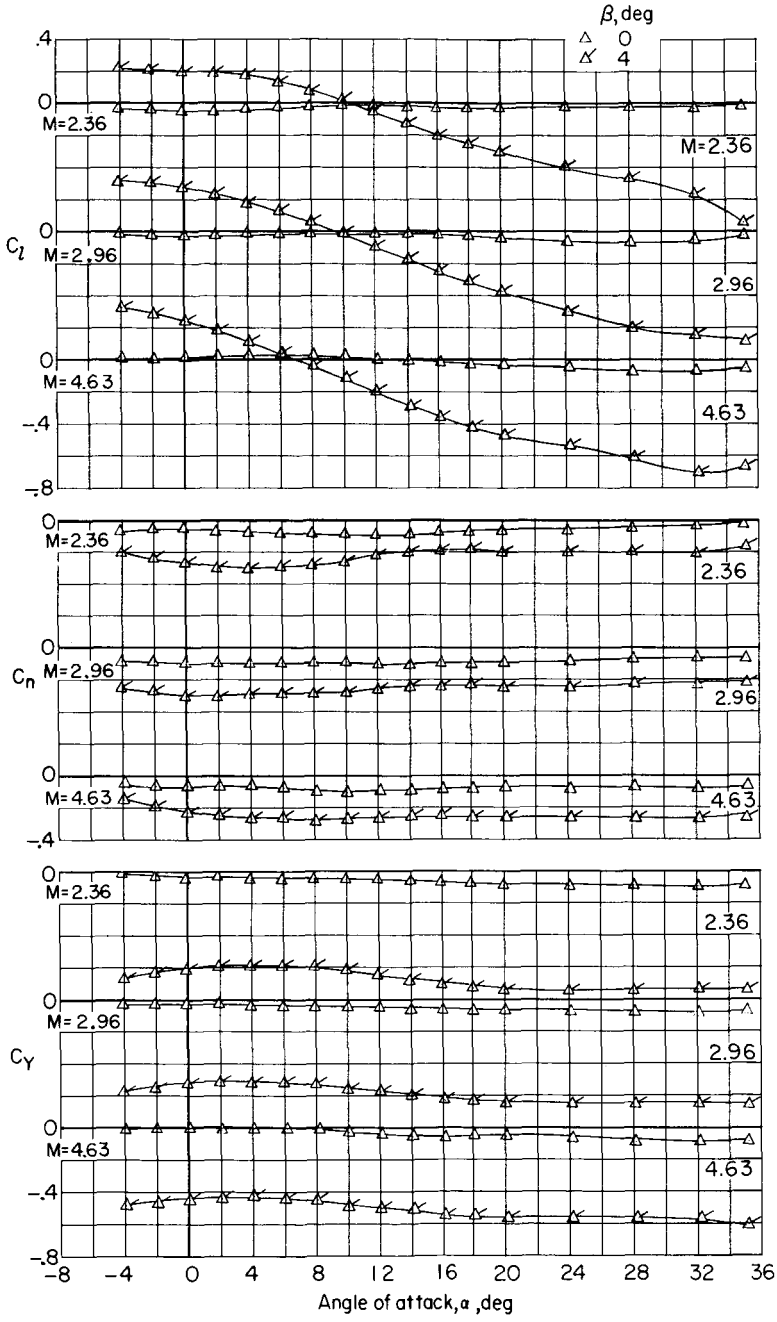

(d) Nacelle on; vertical tails on; $\theta_t = 0^\circ$.

Figure 11.- Concluded.

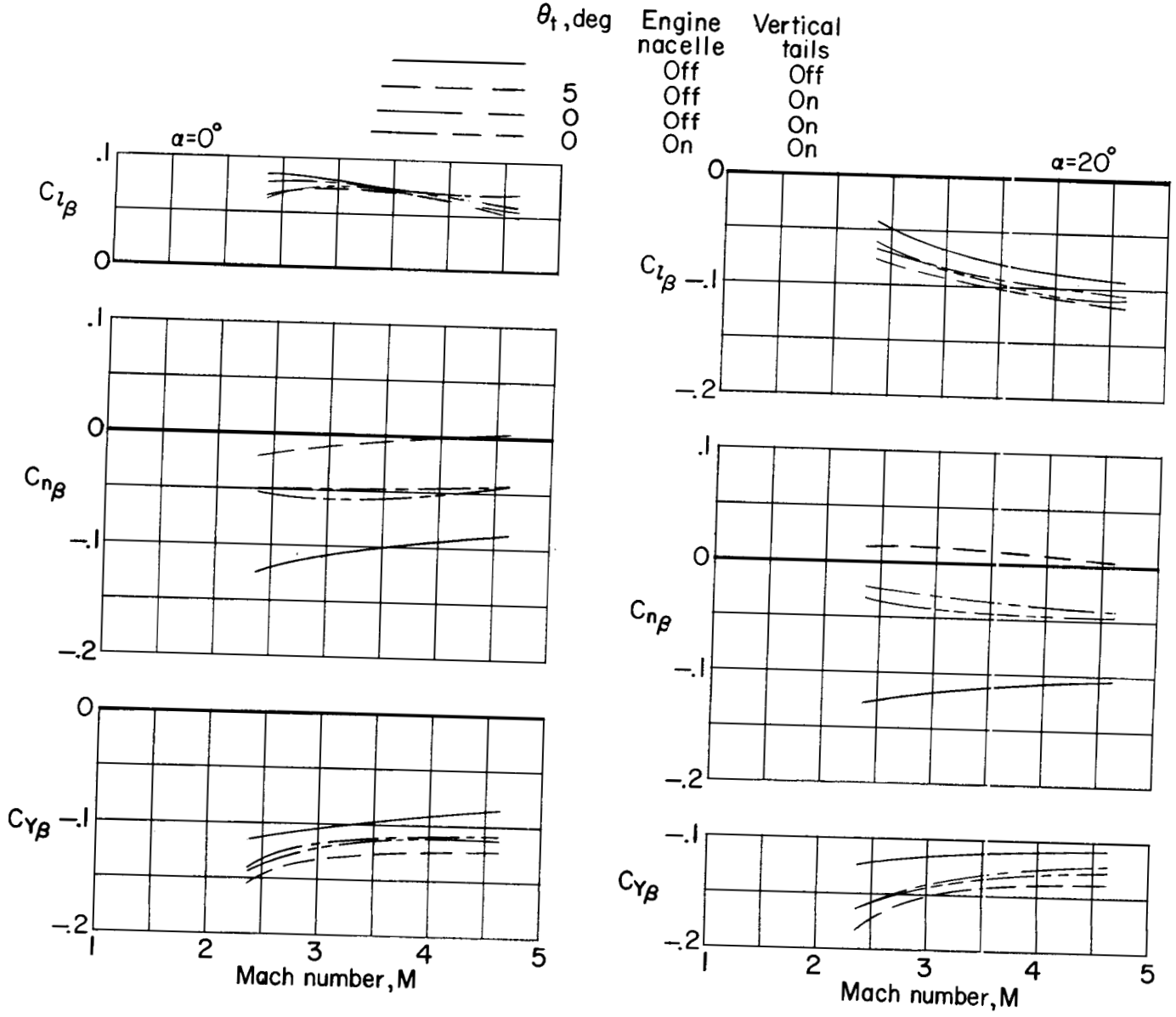

Figure 12.- Variation with Mach number of lateral-directional-stability parameters for first-stage reusable booster. $\theta_c = 15°$.

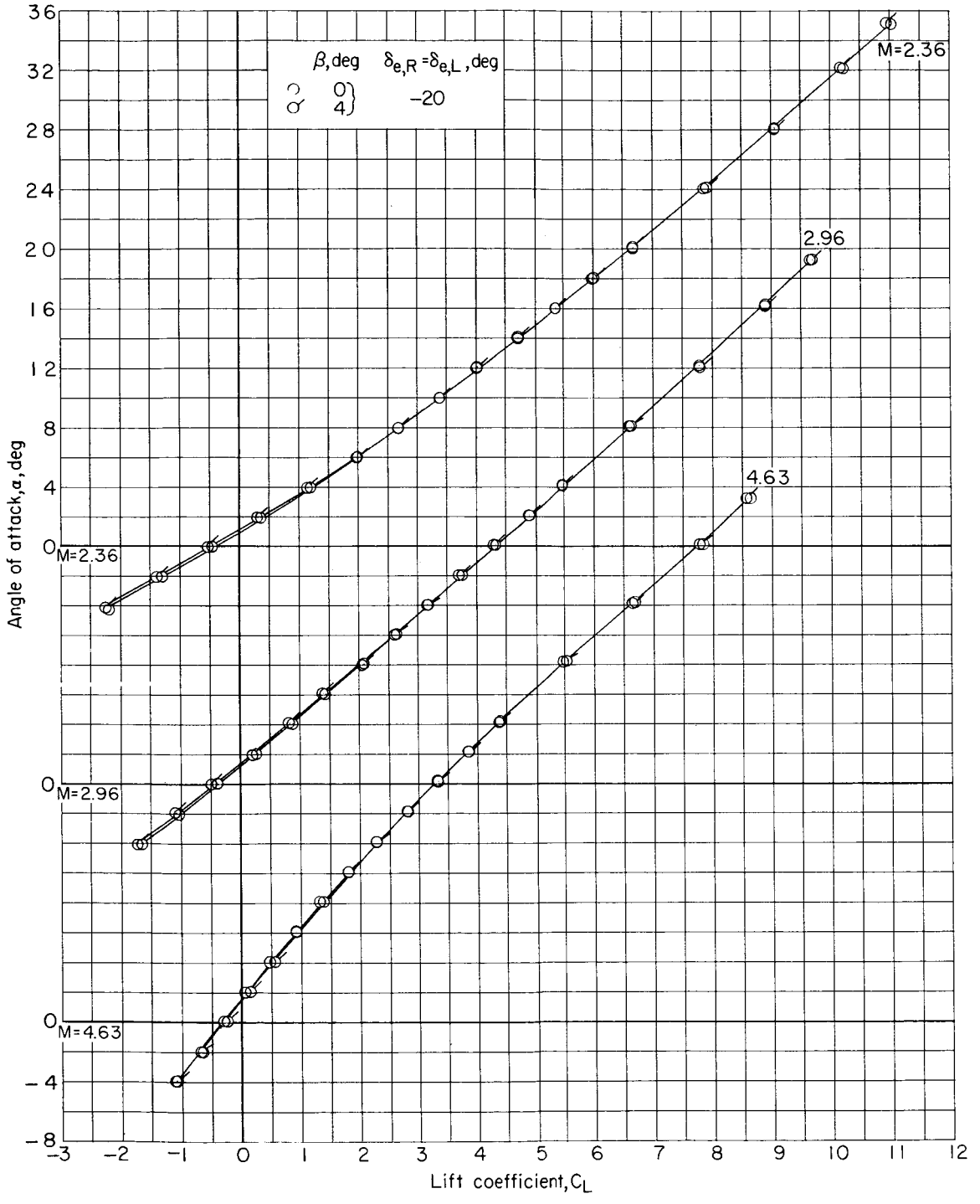

(a) Longitudinal characteristics.

Figure 13.- Aerodynamic characteristics with deflected longitudinal control surfaces of first-stage reusable booster. Engine nacelle off; $\theta_t = 0^\circ$; $\theta_c = 15^\circ$.

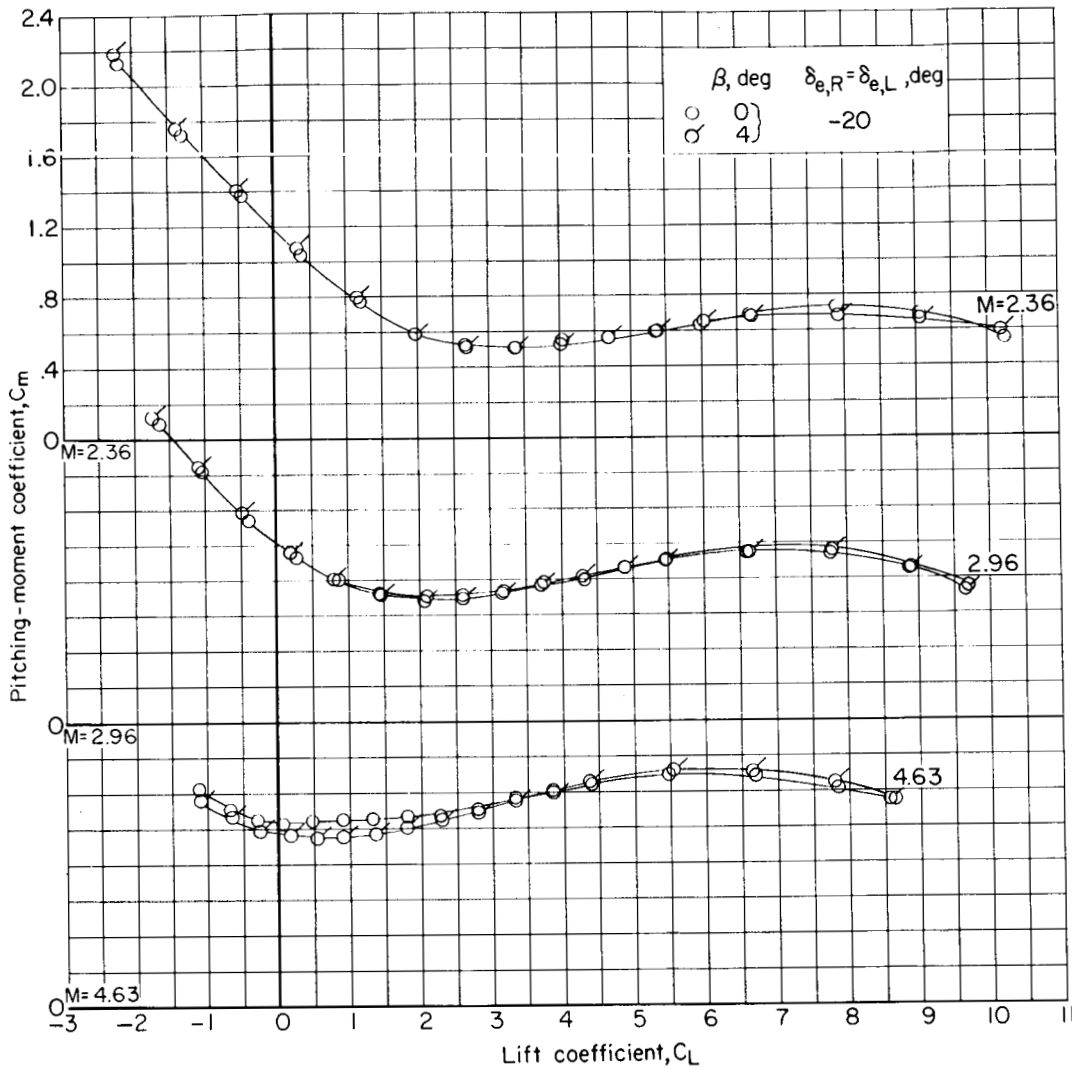

(a) Longitudinal characteristics. Continued.

Figure 13.- Continued.

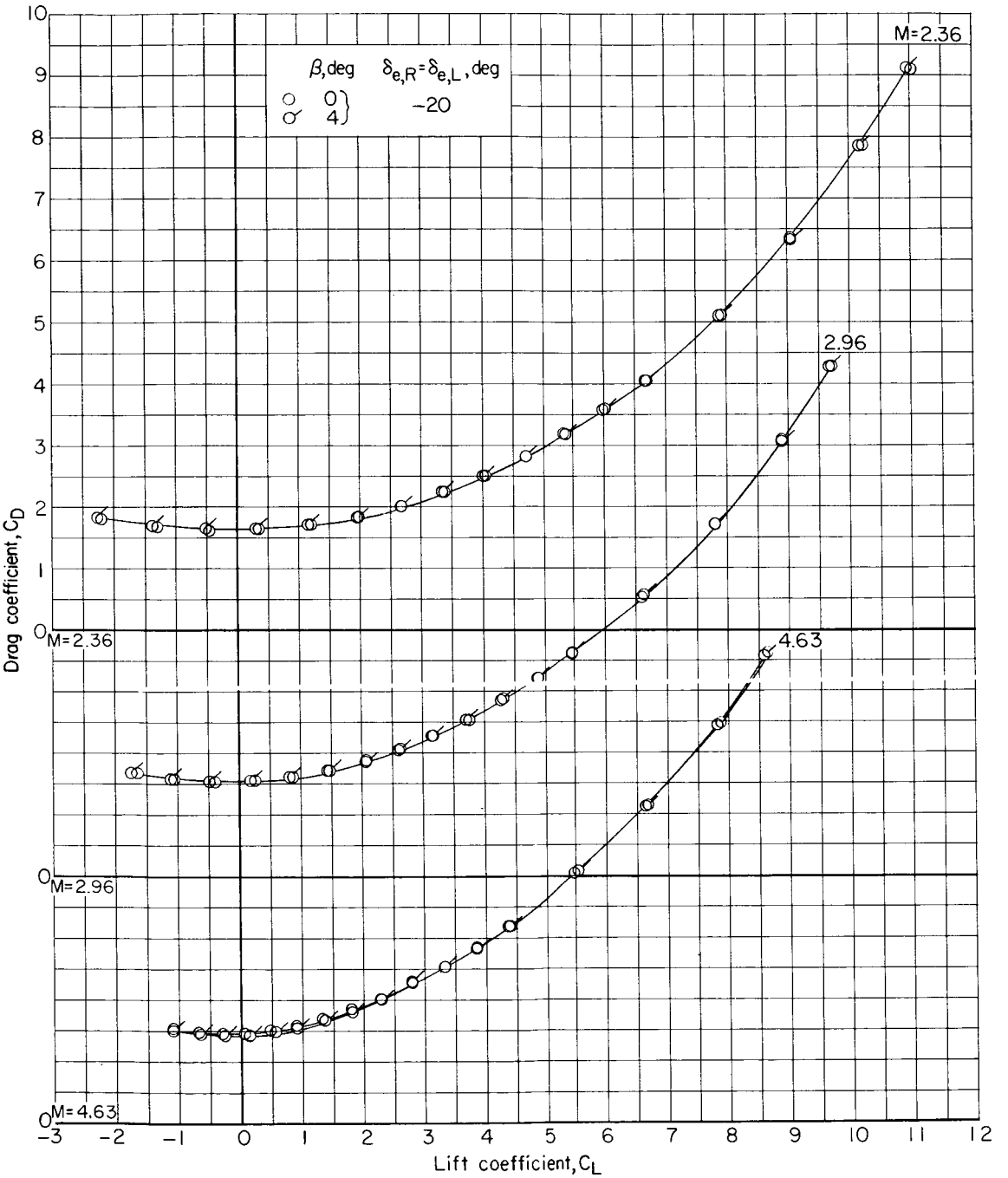

(a) Longitudinal characteristics. Concluded.

Figure 13.- Continued.

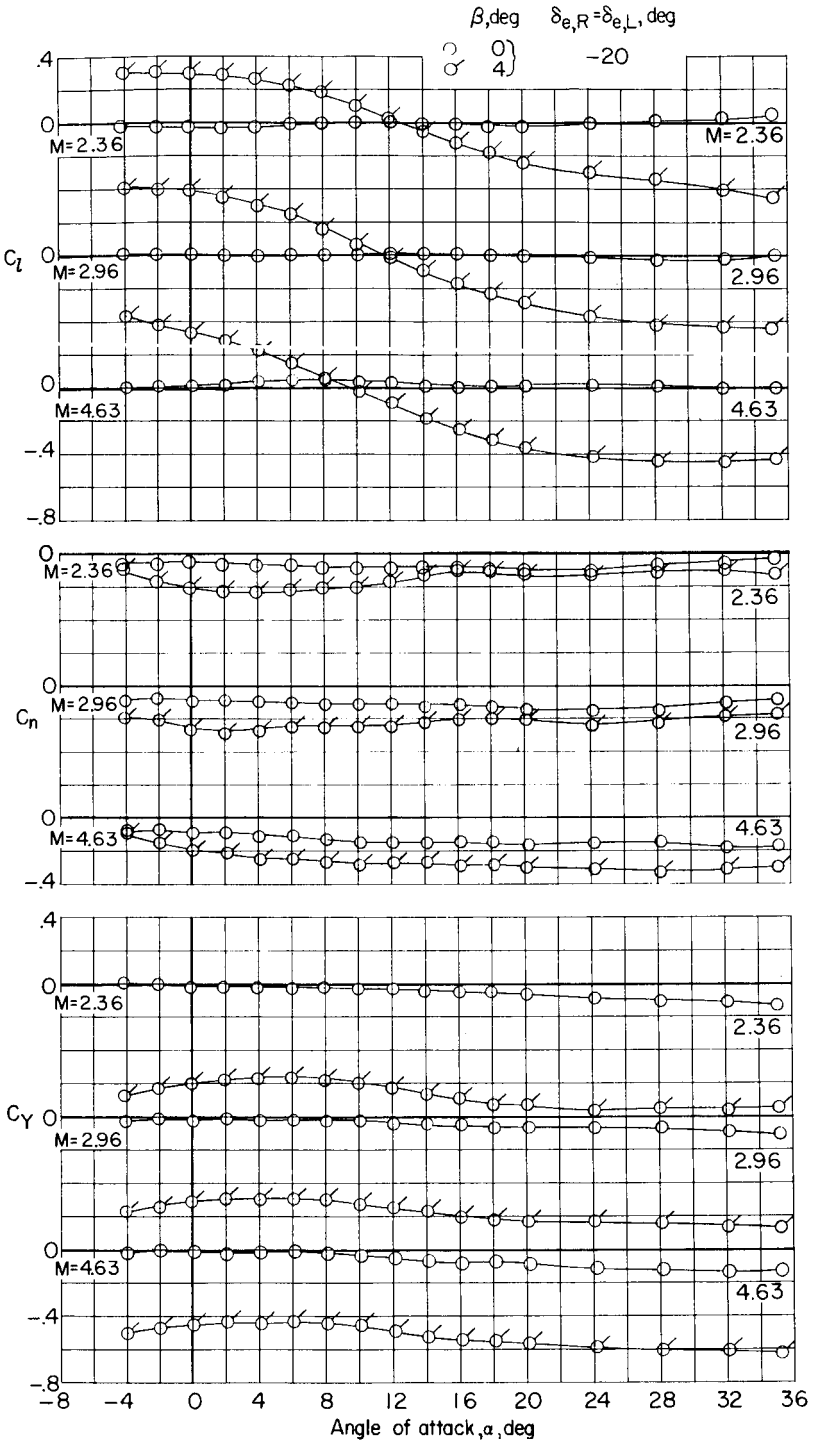

(b) Lateral directional characteristics.

Figure 13.- Concluded.

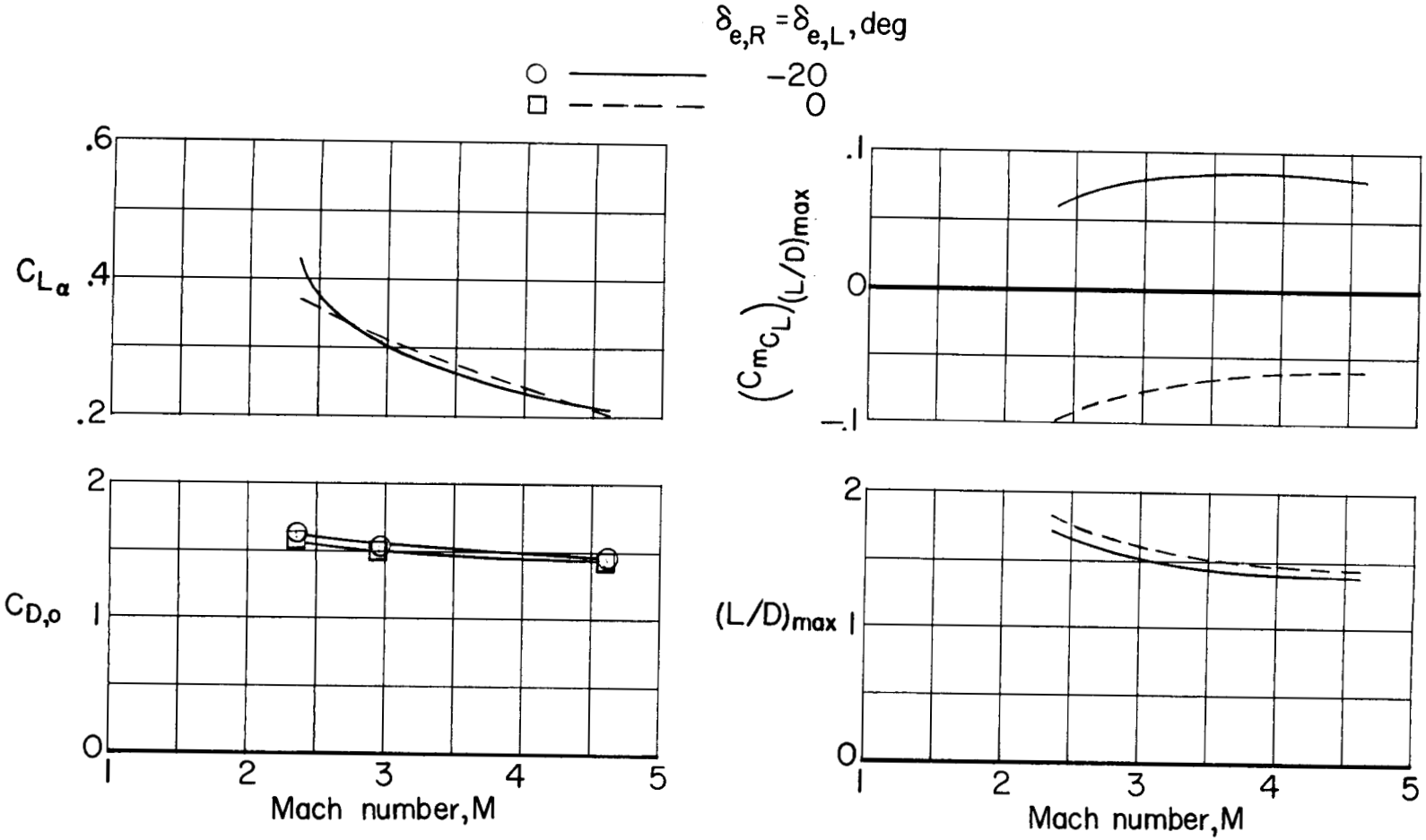

Figure 14.- Variation with Mach number of longitudinal-stability and drag parameters for first-stage reusable booster showing effects of longitudinal control deflections. Engine nacelle off; $\theta_t = 0^\circ$; $\theta_c = 15^\circ$; $\beta = 0^\circ$.

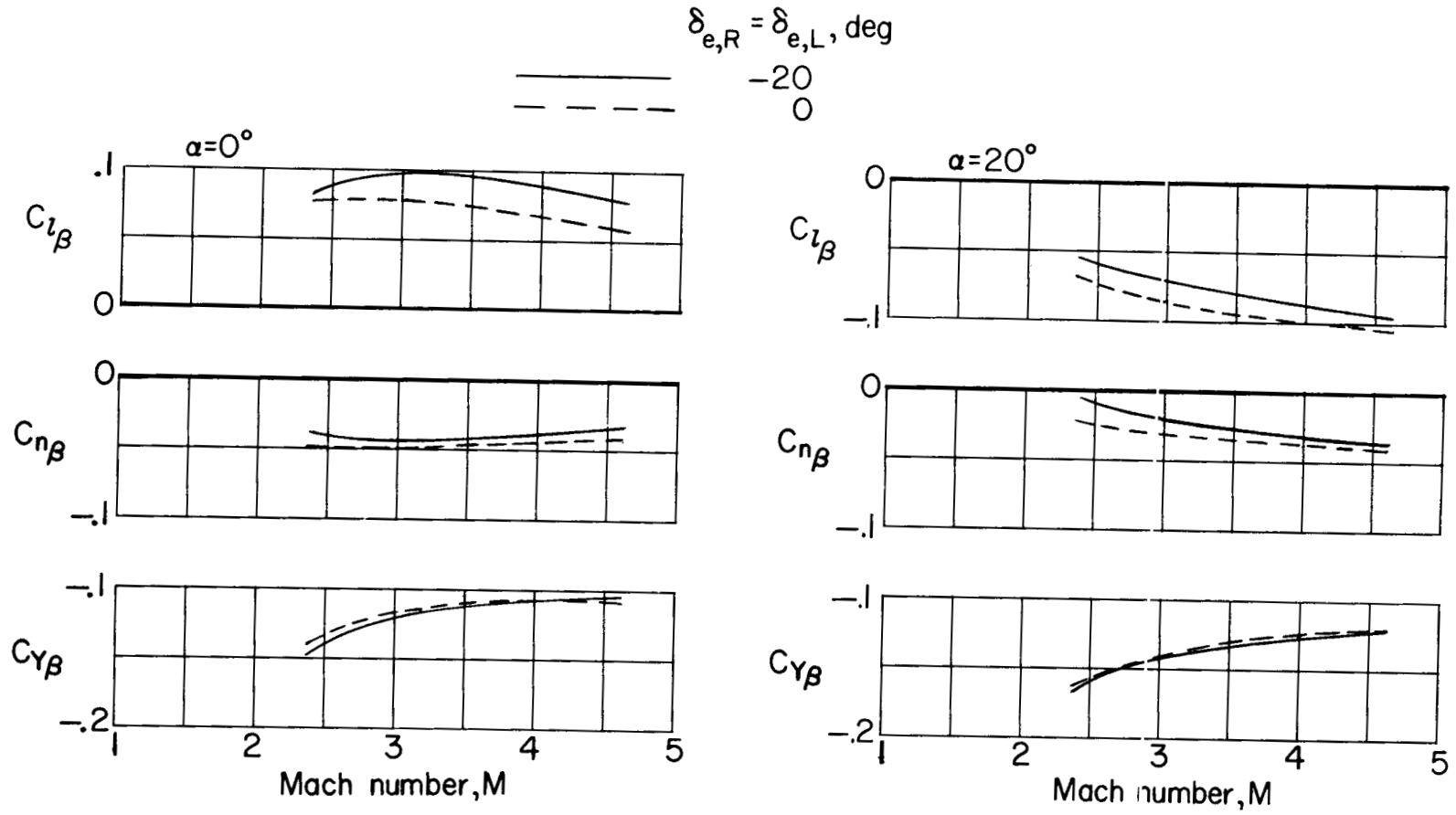

Figure 15.- Variation with Mach number of lateral-directional-stability parameters for first-stage reusable booster showing effects of longitudinal control deflections. Engine nacelle off; $\theta_t = 0^\circ$; $\theta_c = 15^\circ$.

UNCLASSIFIED

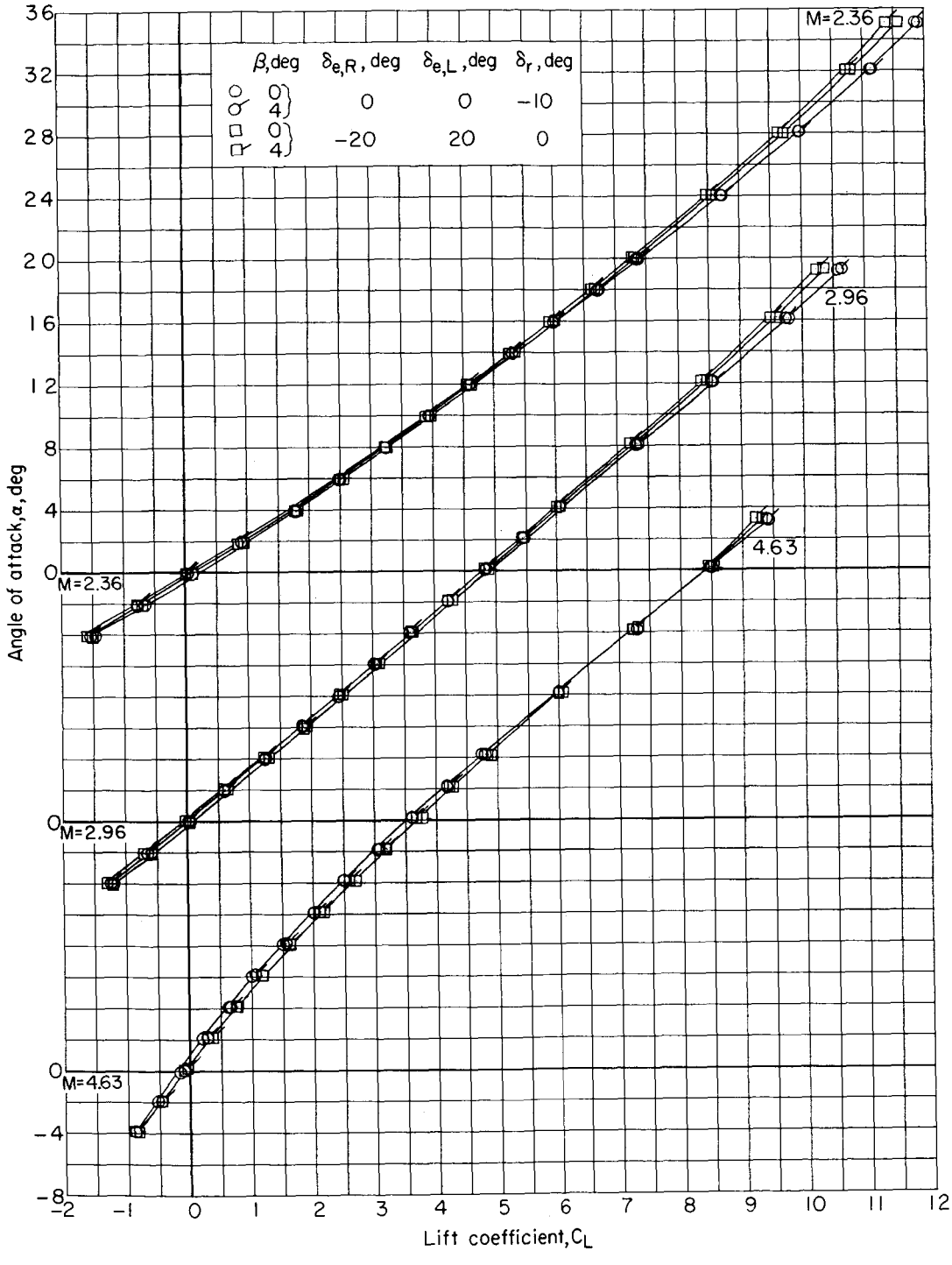

(a) Longitudinal characteristics.

Figure 16.- Aerodynamic characteristics with deflected lateral or directional control surfaces of first-stage reusable booster. Engine nacelle off; $\theta_t = 0^\circ$; $\theta_c = 15^\circ$.

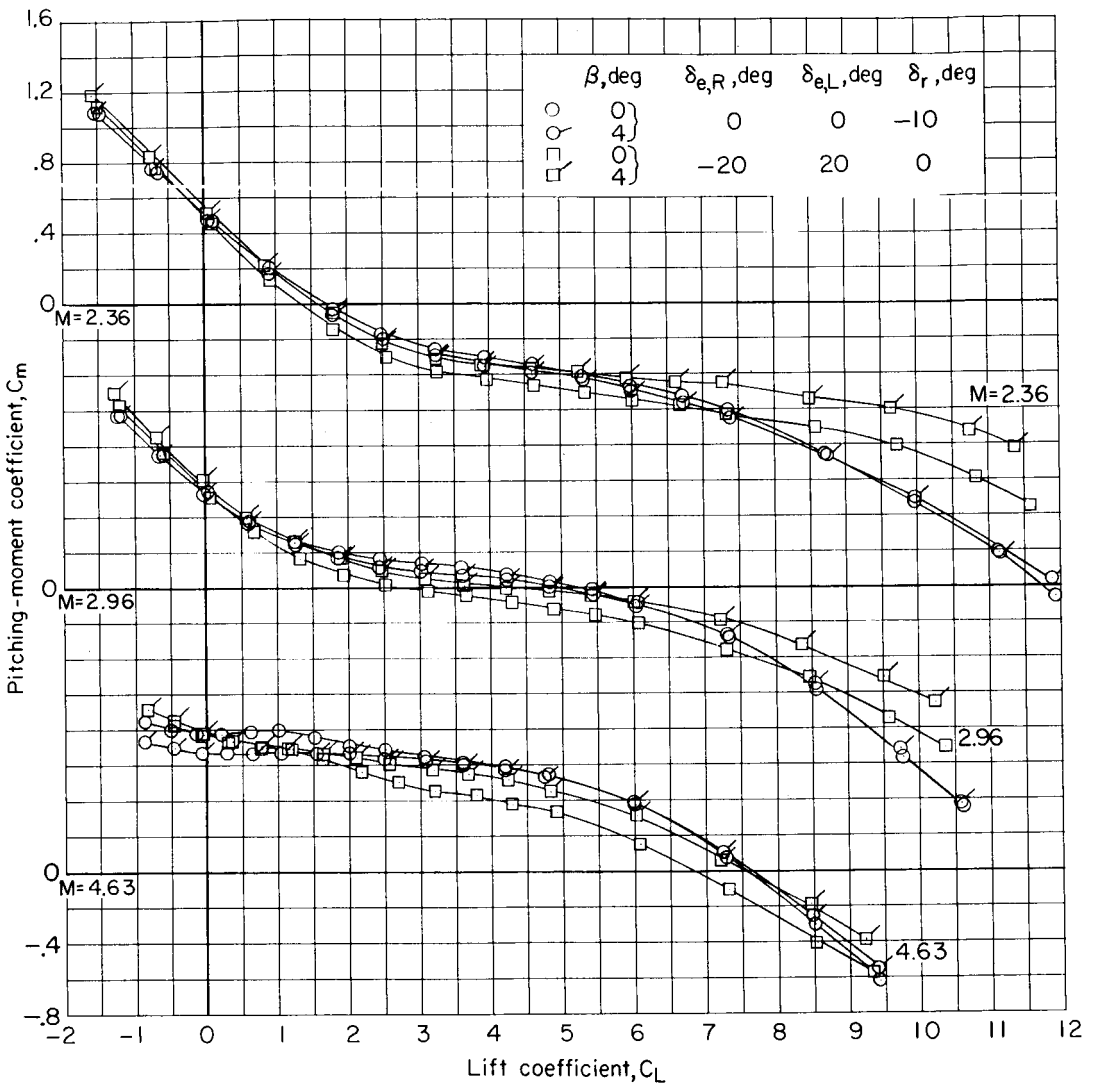

(a) Longitudinal characteristics. Continued.

Figure 16.- Continued.

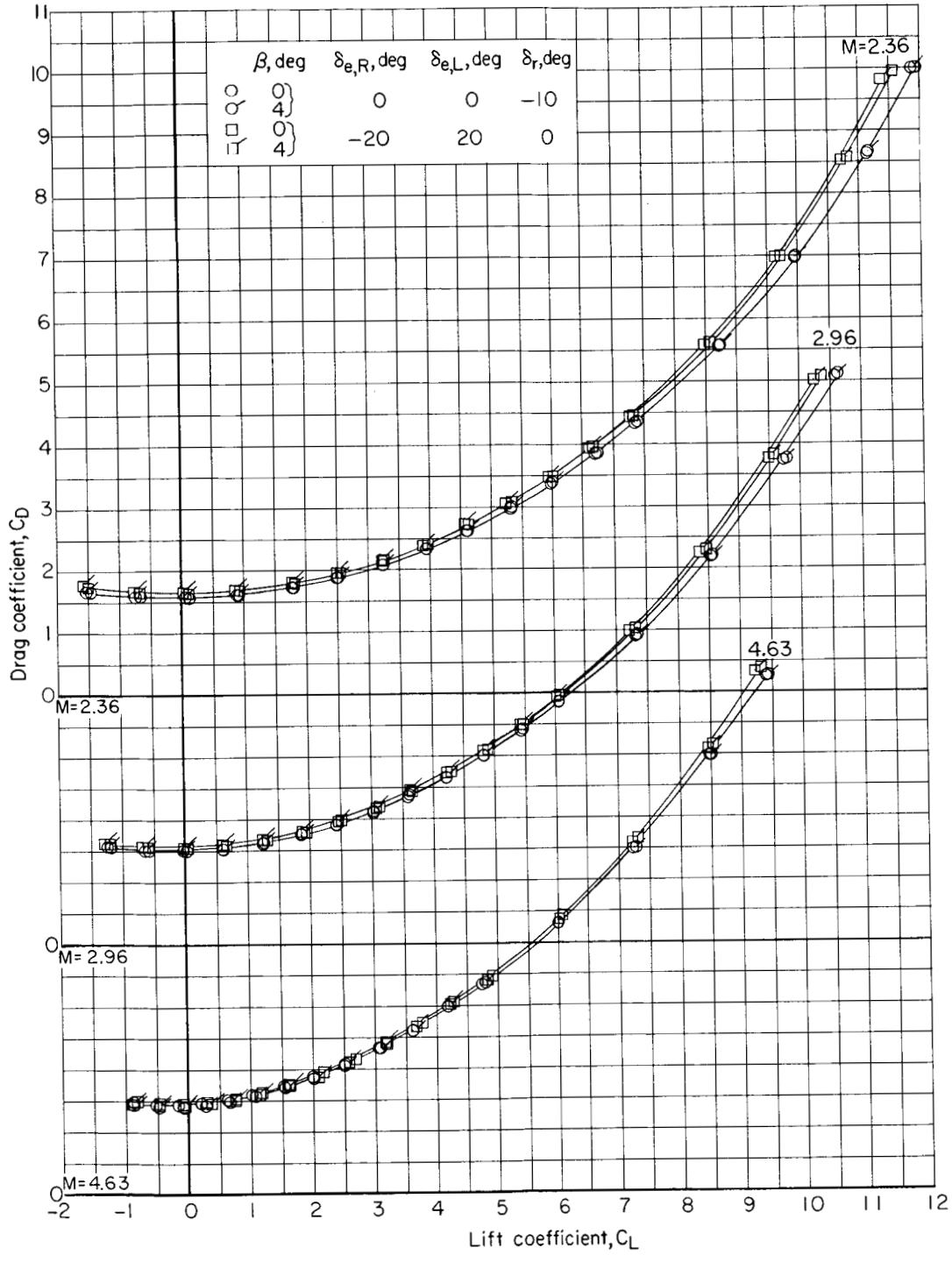

(a) Longitudinal characteristics. Concluded.

Figure 16.- Continued.

(b) Lateral directional characteristics.

Figure 16.- Concluded.

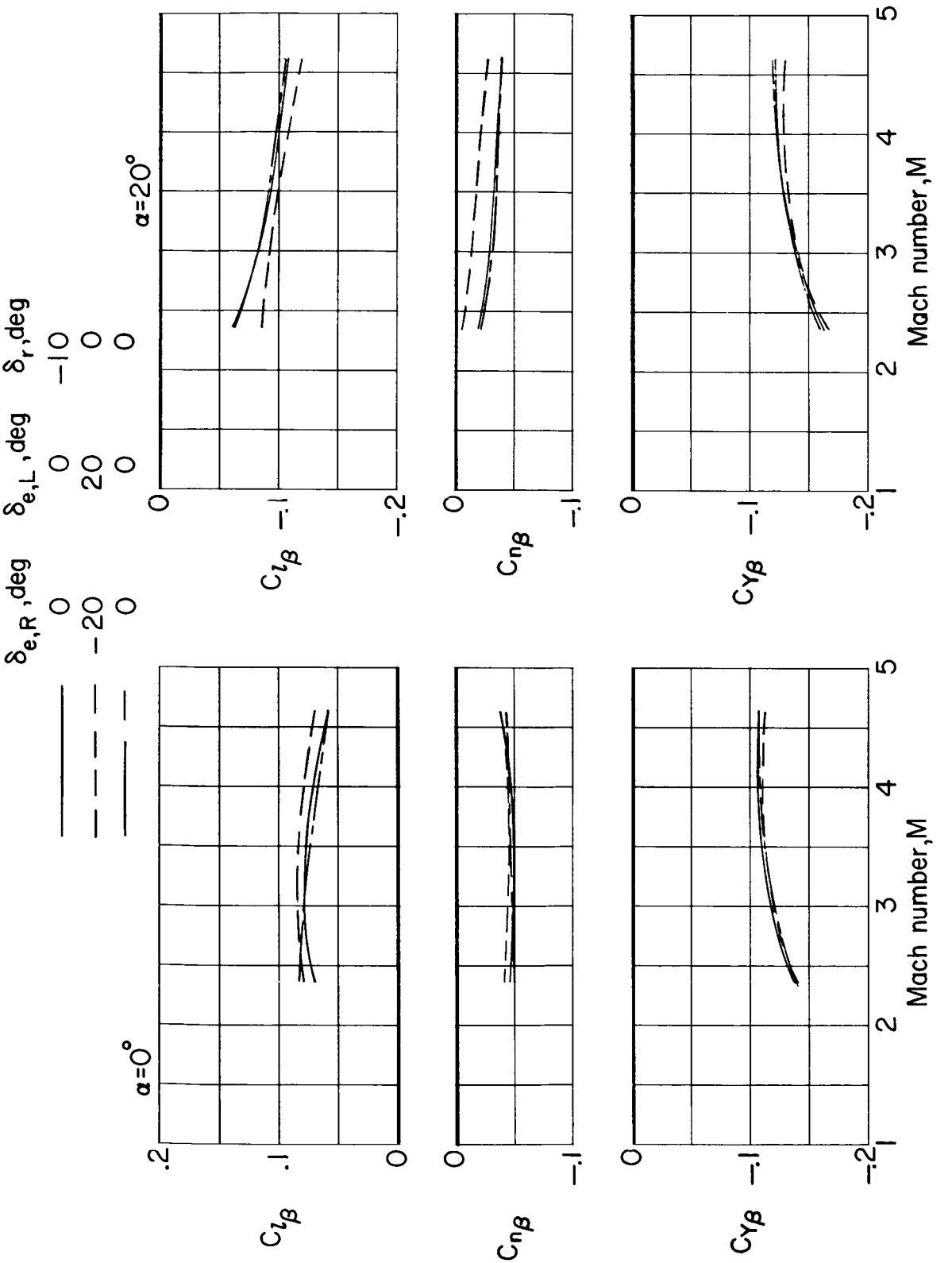

Figure 17.- Variation with Mach number of lateral-directional-stability parameters for first-stage reusable booster showing effects of lateral-directional control deflections. Engine nacelle off; $\theta_t = 0°$; $\theta_c = 15°$.

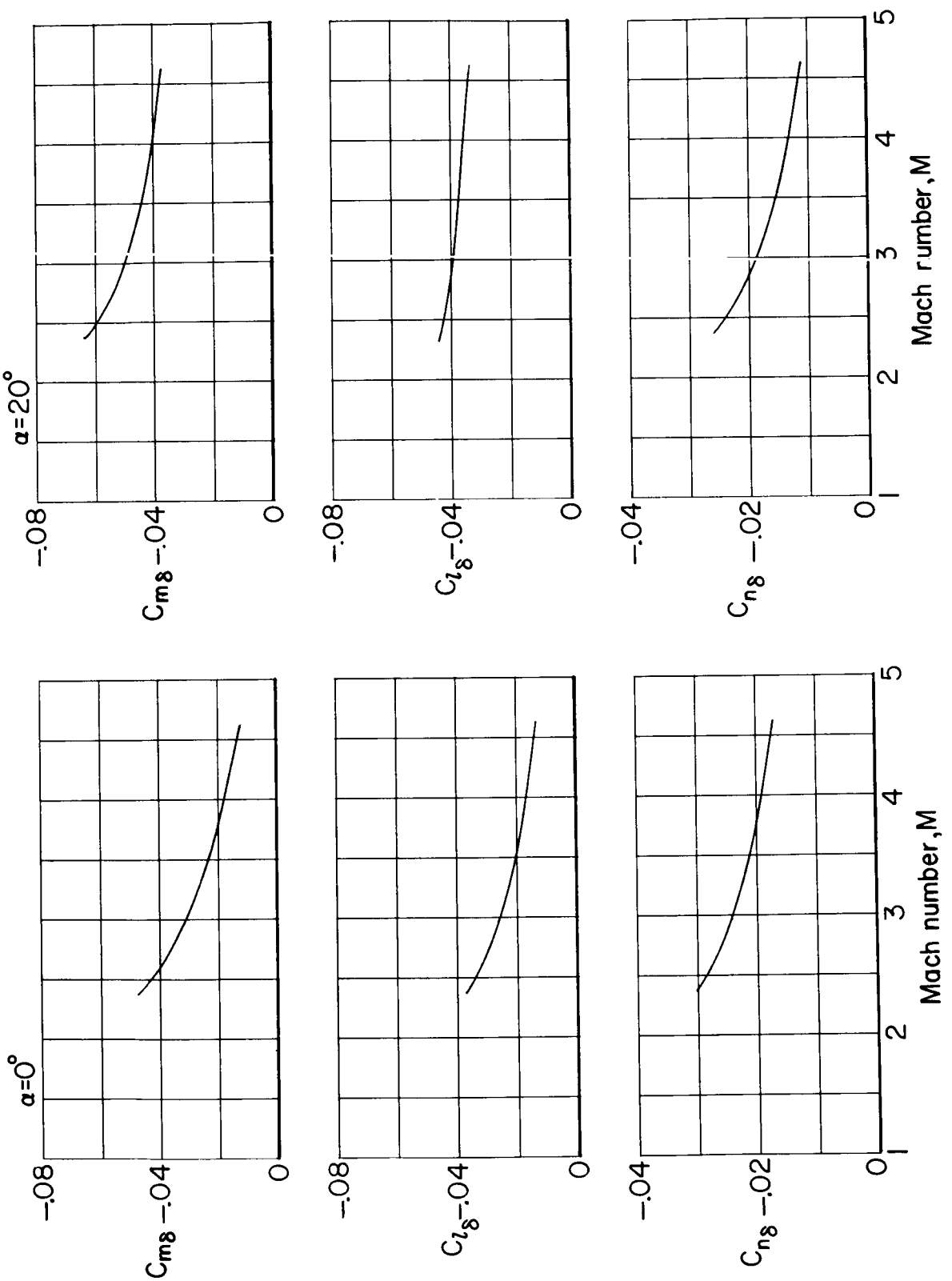

Figure 18.- Control effectiveness of first-stage reusable booster. Engine nacelle off; $\theta_t = 0°$; $\theta_c = 15°$; $\beta = 0°$.

NASA-Langley, 1965 L-4298

"The aeronautical and space activities of the United States shall be conducted so as to contribute . . . to the expansion of human knowledge of phenomena in the atmosphere and space. The Administration shall provide for the widest practicable and appropriate dissemination of information concerning its activities and the results thereof."

—NATIONAL AERONAUTICS AND SPACE ACT OF 1958

NASA SCIENTIFIC AND TECHNICAL PUBLICATIONS

TECHNICAL REPORTS: Scientific and technical information considered important, complete, and a lasting contribution to existing knowledge.

TECHNICAL NOTES: Information less broad in scope but nevertheless of importance as a contribution to existing knowledge.

TECHNICAL MEMORANDUMS: Information receiving limited distribution because of preliminary data, security classification, or other reasons.

CONTRACTOR REPORTS: Technical information generated in connection with a NASA contract or grant and released under NASA auspices.

TECHNICAL TRANSLATIONS: Information published in a foreign language considered to merit NASA distribution in English.

TECHNICAL REPRINTS: Information derived from NASA activities and initially published in the form of journal articles.

SPECIAL PUBLICATIONS: Information derived from or of value to NASA activities but not necessarily reporting the results of individual NASA-programmed scientific efforts. Publications include conference proceedings, monographs, data compilations, handbooks, sourcebooks, and special bibliographies.

Details on the availability of these publications may be obtained from:

SCIENTIFIC AND TECHNICAL INFORMATION DIVISION

NATIONAL AERONAUTICS AND SPACE ADMINISTRATION

Washington, D.C. 20546